# Preface

This dissertation contains work performed in the Polymers and Colloids group of the Cavendish Laboratory at the University of Cambridge from October 2000 to July 2001 under the supervision of Dr. Mark Warner.

The work on the mechanical and optical properties of cholesteric rubbers contained within this thesis represents original research, unless otherwise indicated within the text.

I have not submitted this work for any degree, diploma or similar qualification at this or any other university or similar institution.

I would like to thank the following people, without whom I could not have written this work:

Mark Warner
Eugene Terentjev
Pietro Cicuta
Peter Haynes
Peter Littlewood
Michael Rubinstein
Andrey Dobrynin
Frank and Christine Bermel
Harold Epstein

I would also like to thank the Winston Churchill Foundation for its financial support.

# Contents

# Chapter 1

# Introduction

In this thesis, I develop a general theory for calculating the optical properties of cholesteric liquid crystals, and present the results for several special cases. Cholesteric liquid crystals (CLC's) are one example of a broad class of substances that reflect light, not because of the properties of their constituent molecules, but because of their structure. These materials have come to be known as *photonic crystals*. The tantalising possibility that one can manipulate their structure arbitrarily in order to finely control their optical properties has elicited an enormous amount of interest in the past fifteen years. Conventional crystals have a periodic spacing of atoms, which gives rise to a periodic potential for electrons. Electronic structure theory enables one to calculate band structures which show the energies available to electrons in this system. Analogously, photonic crystals have a periodic dielectric tensor which gives rise to an effective periodic potential for photons. Thus, we can use tools and concepts derived from electronic structure theory to calculate the frequencies available to photons in such media.

Some photonic band structures have frequencies which are not allowed for one or more polarisations. A range of forbidden frequencies is referred to variously as either a stop band or a photonic band gap (PBG). There are several important potential applications for materials with a PBG. One example involves the creation of localised defect modes. If one introduces a small defect into the otherwise periodic structure of a photonic band-gap material, light which is forbidden in the bulk will be confined to the region centered around the defect [1]. Furthermore, within the frequency range defined by the PBG of the bulk, a small defect will only have a small number of additional modes. When used as a laser microcavity, this will prevent spontaneous emission into modes other than the lasing mode, and yield extremely low threshold lasing. Yablonovitch originally estimated that low-threshold continuous-wave lasing could take place at a threshold current density as low as 1 A/cm$^2$ [2]. Recently, microcavities in two-dimensional photonic crystals have been integrated into VCSELs to yield ultra-low threshold lasing experimentally [3]. Alter-

natively, one can design lasers that take advantage of the enhanced dwell time associated with the band edge divergence of the density of states [4]. Experimentally, this band-edge lasing has been observed in cholesteric liquid crystals [5] and cholesteric elastomers [6]. A related application is guiding light around sharp boundaries. If one places a line of defect modes within a photonic band gap material, light may be bent within a distance on the order of one optical wavelength. That turning radius is much shorter than what can be achieved for optical or near-infrared light using total internal reflection. The ability to bend light sharply, and without loss, is crucial for the creation of an optical integrated circuit, a device which would lie at the heart of any future optical computing systems. One major potential use for optical computing is switching in telecommunications systems. Translating optical signals arriving via fibre-optic cables into electronic signals and back constitutes a substantial overhead in current industry-standard technologies, such as SDH/SONET cross connects for basic TDM circuit switching [7]. All-optical processing would alleviate this bottleneck, leading to decreased latency.

The earliest research in photonics was concerned with manufacturing materials that have a three-dimensional photonic band gap in the microwave spectrum [2, 8, 9, 10]. This goal proved to be more elusive than initially thought. While Yablonovitch and Gmitter thought they had manufactured a material with such a total-gap [10], it turned out to be a pseudo-gap with a low but non-zero density of states, as pointed out explicitly in the theoretical calculations of several groups [11, 12, 13]. Shortly afterwards, Yablonovitch and colleagues were able to fashion a structure with a full photonic band gap, now dubbed Yablonovite [14]. Later, Ozbay and co-workers designed a picket fence structure which is assembled by stacking two-dimensional layers [15].

Nonetheless, those techniques have proven difficult to extend to optical wavelengths for several reasons. First, the usefulness of photonic crystals is heavily dependent on perfect periodicity – slight misalignments tend to destroy photonic band gaps. Furthermore, the feature size of a photonic crystal must be no larger than one wavelength in the medium, or otherwise all polarisations and phases of light will experience a smooth dispersion relation (and thus no gaps). This challenge is compounded by the fact that the maximum feature size decreases as the refractive index contrast of a photonic material increases. Clearly, the smaller the features, the greater the challenge that precise alignment presents. That has made microfabrication of photonic crystals that have band gaps at near-infrared or optical frequencies a particularly challenging proposition.

Recently, there has been an increased interest in self-assembling PBG systems because they have the potential to overcome the problem of scale in a clever way. If one chooses the right materials and parameters for a precise, self-assembling system, a photonic crystal should emerge automatically without any need for expensive microfabrication tech-

niques, such as photolithography. Researchers have devised several systems which have the potential to meet the criterion of forming a precise, periodic array with sufficient refractive index contrast. Examples include air holes in a titania matrix [16], copolymer-homopolymer films which form lamellar structures [17], thin films of PMMA infilled with $SnS_2$ [18], and cholesteric liquid crystals (CLC's) [5, 6, 19, 20].

In this thesis, I investigate the optical properties of CLC's. A CLC has local orientational ordering along a director $\mathbf{n}$, which rotates as a periodic function of distance along the pitch axis $z$, as illustrated in figure 1.1. The director of an ideal CLC advances uniformly, tracing out a helix of pitch $p_0$. The pitch can be adjusted to match the wavelength of visible light, whereupon a number of spectacular optical effects are observed experimentally and explained theoretically [19, 20]. In particular, in experiments conducted at normal incidence, circularly polarised light which twists in the same sense as the helix is reflected with its original polarisation, while circularly polarised light that twists in the opposite sense is transmitted unchanged. By contrast, a normal mirror will reflect either handedness with the opposite polarisation that it initially had. A CLC can be considered locally uniaxial, with a dielectric permittivity $\epsilon_\parallel$ along $\mathbf{n}$ and $\epsilon_\perp$ perpendicular to $\mathbf{n}$. By solving Maxwell's equations in a rotating frame, de Vries found a single band gap in the photonic structure of an ideal CLC at normal incidence [19].

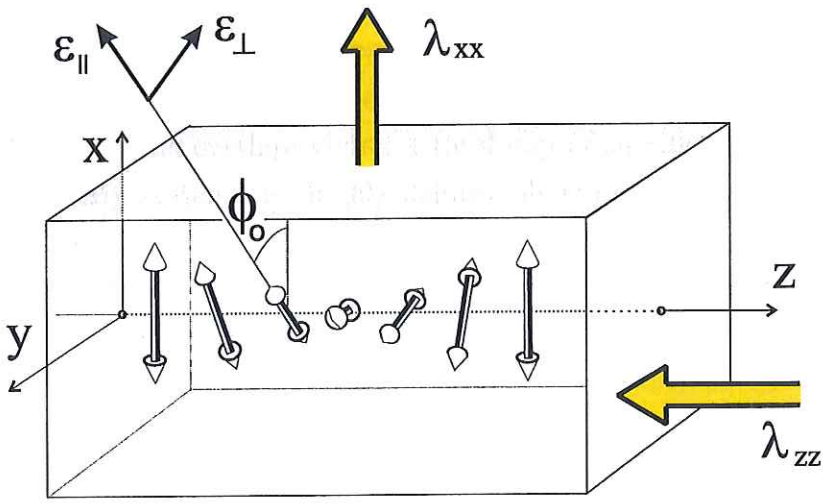


Figure 1.1: Schematic diagram of a cholesteric liquid crystal. The director twists periodically along the pitch axis, which corresponds to the $z$ axis here. The CLC is also optically uniaxial, with a dielectric constant $\epsilon_\parallel$ along the direction of nematic order, and dielectric constant $\epsilon_\perp$ in the plane perpendicular to the nematic order. For future reference, elements of the deformation gradient tensor $\underline{\underline{\lambda}}$ are shown: $\lambda_{xx}$ is a stretch applied in the $x$-direction, and $\lambda_{zz}$ is the attendant contraction along $z$.

The recent theoretical prediction of and experimental creation of cholesteric rubbers has revived interest in the optics of CLC. Nematic rubbers were first created in the lab by Finkelmann in 1981 [21]. More recently, it has been shown that polymeric liquid crystals can be cross-linked into cholesteric elastomers (CE's) which retain cholesteric order [22]. Furthermore, these elastomers have been shown to be monodomain, with a spontaneous and uniform orientation of the helical structure. Warner and colleagues have predicted how the helical structure will change under two different types of strain, given the simple assumptions of affine deformation and strong anchoring [23]. These cholesteric elastomers are significant because, like regular CLC's, they have a band gap for one polarisation of light, but additionally, they are tunable. That means that the applications mentioned before, such as low-threshold lasing and light bending, can work not just at one predetermined target frequency, but a whole range of frequencies, using the fairly simple control mechanism of mechanical stretching.

At this point, one might seek to employ de Vries' method of transforming to a rotating coordinate frame to characterise the optical properties of cholesteric elastomers. However, as I show in section 4.2, his approach is intractable when the director helix no longer advances uniformly, as is the case for a CE under strain. Thus, I present a new method in chapter 5 that is computationally tractable and successfully describes the new and deforming photonic bands that I have discovered. My calculations point to new phenomena and new applications, not possible in existing photonics and hitherto unsuspected in the liquid crystal field. For instance, I find multiple gaps, some not at the zone edges, in contrast to classical CLC's. I also observe gaps for light of the opposite handedness to the underlying helix, again unexpected in classical CLC systems. At some points the gaps for both polarisations overlap, giving a total gap of significance when polarisation control is required. My systems are highly deformable (to many 100s%) and I shall find shifts in the (developing) band structure that can be large.

Existent photonic media typically have piecewise variation of an isotropic refractive index in going between a matrix and its inclusions. By contrast, CLC's have a continuous variation of the principal axes of birefringence. Polarisation effects are thus very subtle and become more so for oblique incidence. Control of polarisation is at the heart of LC and optical devices; I thus view this work as a first step toward creating and understanding new classes of photonic solids with deformable, tunable band structures.

In this thesis, I proceed as follows. First, I discuss how liquid crystalline order comes about and the elastic response of a liquid crystal, focusing on the structure of a CLC along with its behaviour under an external field. Next, I review the theory of isotropic rubbers, then explain the phenomenon of nematic rubbers, which bring together liquid crystal and rubber theory in a novel way. Then I calculate the optical properties of the model system

developed in the previous two chapters. I recapitulate de Vries' approach and results, and show the limits of his technique for the more generalised problems of distorted cholesteric helices or oblique incidence. I then overcome this methodological deficiency by applying the modern formalism of photonics, as originally developed by Ho, Chan and Soukoulis [11] and refined by Meade and colleagues [24]. I develop equations appropriate for solving the problems of light normally or obliquely incident upon a distorted helix. I conclude by presenting my results for normal and oblique incidence in a one-dimensionally periodic cholesteric medium.

# Chapter 2

# Liquid Crystal Theory

## 2.1 Overview

Liquid crystals can be viewed as a state of matter intermediate between the liquid and solid phases. There are at least five main types of liquid crystals: nematics, cholesterics, smectics, columnar phases and blue phases. All five demonstrate orientational ordering, made possible by the nature of the building blocks characteristic of liquid crystals, idealised as long, thin, rigid rods, pointing in a particular direction, which are generally referred to as mesogens. These mesogens generally have anisotropic electromagnetic properties, such as their dielectric constants. When mesogens are organised into a periodic structure, their anisotropy can give rise to singular optical properties. Except for the nematic phase, there is generally a periodicity in the structure as well as a dielectric anisotropy that may combine and give rise to singular optical properties.

The first phase transition for achiral liquid crystals is the nematic-isotropic transition. Mesogens in the isotropic phase have a uniform angular distribution, whereas in the nematic phase, there is a bias in their angular distribution, even though both phases lack translational order (just as in an ordinary liquid). Entropy favours an isotropic state, but other interactions encourage the creation of a nematic phase. First, there are hard steric repulsions that favour alignment. The strength of these interactions increases with concentration. Liquid crystals which make a transition from the isotropic to nematic phase with an increase in concentration are known as lyotropic liquid crystals. Also, there are soft anisotropic forces that tend to favour the alignment of nematic subunits. These forces generally dominate over entropy at lower temperatures. At a certain temperature, known as the isotropic-nematic transition temperature, there will be a first-order phase transition between the two states. Liquid crystals which experience these transitions are known as thermotropic liquid crystals.

One can construct a Ginsburg-Landau (GL) mean-field theory which captures the

essential features of the thermotropic phase transition by writing down an energy and entropy in terms of an order parameter, a dimensionless measure of the degree of order in a system. In general, the order parameter in a GL theory is chosen so that it will vanish on the less-ordered (isotropic) side of the transition, and be "small" in some sense on the other side in the vicinity of the phase transition, so that I need only to keep the lowest-order terms required by symmetry and general constraints on a physical potential in my expansion of the free energy.

## 2.2 Order Parameter

Based on the nature of the liquid-crystalline subunits, it is evident that the order parameter will be in terms of the orientations of the individual rods with respect to the average direction. The average direction in which the rods point in a small sphere about a position $\mathbf{r}$ is a unit vector, $\mathbf{n}(\mathbf{r})$. If a given rod $\alpha$ in that region has an orientation $\mathbf{v}_\alpha(\mathbf{r})$, then the relative orientation can be parameterised by $\mathbf{n}(\mathbf{r}) \cdot \mathbf{v}_\alpha(\mathbf{r}) = \cos\theta_\alpha$.

I would like to decompose the distribution of $\{\cos\theta_\alpha\}$ in terms of moments. By analogy with quantum mechanics, I can choose Legendre polynomials, generally denoted by $P_l(\cos\theta)$. They capture multipole moments sequentially, since $P_l$ corresponds to the $l^{\text{th}}$ moment. They also have the desirable property of normalisation, since $\forall_l\ P_l(1) = 1$, and orthogonality, since $\int_{-1}^{1} \mathrm{d}x\ P_l(x)P_{l'}(x) = \frac{2}{2l+1}\delta_{ll'}$.

The first non-trivial choice is the dipole moment $\langle P_1(\cos\theta)\rangle = \langle\cos\theta\rangle$. However, the heads and tails of liquid crystal subunits are equivalent, either because they have a center of inversion or at least an equal probability of pointing parallel or anti-parallel in a given direction. As a result, there will be an equal contribution from $\mathbf{v}_\alpha$ and $-\mathbf{v}_\alpha$, which yield $\cos(\theta_\alpha)$ and $\cos(\pi - \theta_\alpha)$, respectively. These are equal but opposite contributions, which tells us that $\langle P_1(\cos\theta)\rangle = 0$ for *any* distribution of rods, from isotropic to perfect ordering, i.e., $\forall_\alpha\ \theta_\alpha = n_\alpha\pi + \phi$, where $n_\alpha$ is an integer, and $\phi$ is an arbitrary but constant phase. The next choice is the quadrupole moment $\langle P_2(\cos\theta)\rangle = \left\langle \frac{1}{2}\left(3\cos^2\theta - 1\right)\right\rangle$. Unlike before, contributions to the quadrupole moment from $\mathbf{v}_\alpha$ and $-\mathbf{v}_\alpha$ will be equal in magnitude and direction, which means that the quadrupole moment may be non-vanishing in general for a liquid-crystalline system. Thus, the degree of order $S$ is usually defined as $S = \langle P_2(\cos\theta)\rangle$. Furthermore, an isotropic distribution, $\mathcal{P}(\theta_\alpha) = \frac{1}{2\pi}$, yields $S = 0$, while a perfectly ordered distribution yields $S = 1$. A small degree of ordering will lead to a small value of $S$ ($S \ll 1$), thus meeting my criterion for an order parameter.

Nonetheless, there is one additional complication. Right now, I only have one parameter that would be the same under any overall rotation of the axes. I want to define a second-rank tensor that captures the orientation of the order. I call this tensor $Q_{ij}$ and

initially guess that it will go as $Q_{ij} = Sn_in_j$, so that it will be oriented along the direction of the local nematic order. However, since my system has only quadrupolar order, I follow the convention that $Q_{ij}$ should be traceless. As a result, I rewrite

$$Q_{ij} = S\left(\frac{3}{2}n_in_j - \frac{1}{2}\delta_{ij}\right) . \tag{2.1}$$

If I were to choose a coordinate system such that $\mathbf{n} = \hat{x}$, then my tensor would be given explicitly by

$$Q_{ij} = \begin{pmatrix} S & 0 & 0 \\ 0 & -\frac{1}{2}S & 0 \\ 0 & 0 & -\frac{1}{2}S \end{pmatrix} . \tag{2.2}$$

## 2.3 Ginzburg-Landau Model

Given an expression for the liquid crystalline order, I can now construct a GL free energy. I start with the observation that the free energy, being a scalar quantity, should be invariant under all rotations. As a result, the expansion of the free energy of a nematic LC will be in terms of the traces of the various moments of $Q_{ij}$. The series begins with the second order, because $Q_{ii}$ is zero by definition, and has the first three terms,

$$F = aQ_{ij}Q_{ji} + bQ_{ij}Q_{jk}Q_{ki} + cQ_{ij}Q_{jk}Q_{kl}Q_{li} . \tag{2.3}$$

For a uniaxial[†] system, such as the one implied by equation (2.2), I can rewrite the free energy expression, equation (2.3), in terms of the scalar order parameter $S$, which yields

$$F = rS^2 - wS^3 + uS^4 , \tag{2.4}$$

where each of the coefficients $r, w,$ and $u$ are just proportional to the corresponding coefficients of equation (2.3).

Quite generally, any free energy of the form given in equation (2.4) must be bounded from below, so it is assumed that $u > 0$. It is conventional to assume that the second-order coefficient $r$ is linear with temperature, so that $r = a(T - T^*)$, where $T^*$ is a crossover temperature. In the case where $w = 0$, this corresponds to a system which will have a minimum energy at $S = 0$ for $T > T^*$ and $S \neq 0$ for $T < T^*$, and leads to a second-order phase transition. The more interesting case is when $w > 0$, which gives rise to a first-order phase transition. The order parameter and the critical temperature at which the nematic-isotropic transition takes place can be calculated as follows. First, the critical values of

[†]The order parameter of section 2.2 has cylindrical symmetry, and thus, is uniaxial.

the free energy given in equation (2.4) can be found by setting the first derivative of $F$ to zero, so that,

$$\frac{\partial F}{\partial S} = 2rS - 3wS^2 + 4uS^3 = 0 \,. \tag{2.5}$$

Second, the energies of the ordered and unordered states must be equal – since the disordered state has zero energy by definition, it is also required that

$$rS^2 - wS^3 + uS^4 = 0 \,. \tag{2.6}$$

Solving equations (2.5) and (2.6) simultaneously yields a pair of values for the phase transition: $r_c = w^2/4u$ and $S_c = w/2u$. This value of $S$ represents a discontinuous jump from zero, corresponding to a first-order transition. Given that the transition temperature $T_c$ is close to $T^*$, GL theory represents a good approximation to the actual phase transition.

## 2.4 Generalised Elasticity

Given that a LC has locally nematic order, one might wish to consider how the director field, $\mathbf{n}(\mathbf{r})$, varies over space. Observations suggest that $\mathbf{n}(\mathbf{r}) = \mathbf{n} = \text{const}$ is the minimum energy state. Of course, deviations away from a constant $\mathbf{n}(\mathbf{r})$ should still be allowed for all liquid crystalline systems, and will occur at any non-zero temperature and for some boundary conditions. The goal of the generalised theory of elasticity is to construct the most general possible free energy from combinations of vector operators acting on $\mathbf{n}(\mathbf{r})$. I expect the free energy to be a scalar or pseudoscalar quantity which I can expand in powers of the gradient of $\mathbf{n}$, i.e., $\nabla\mathbf{n}$. If a non-constant $\mathbf{n}$ were a minimum energy state, I'd expect there to be a scalar term linear in $\nabla\mathbf{n}$. The first possibility that's invariant under rotations is $\nabla \cdot \mathbf{n}$. However, this term changes signs under the transformation $\mathbf{n} \to -\mathbf{n}$. Since $\mathbf{n}$ and $-\mathbf{n}$ are indistinguishable in a liquid crystal, the $\nabla \cdot \mathbf{n}$ term must vanish. The only other possibility is $\mathbf{n} \cdot (\nabla \times \mathbf{n})$, but this changes sign under a parity transform – so for a centrosymmetric system, this term must also vanish (e.g., a regular nematic LC). In that case, the first non-vanishing term will go as $(\nabla\mathbf{n})^2$. In the case where variations are slow compared to molecular lengths, i.e., $a\nabla \cdot \mathbf{n} \ll 1$, this leading term will dominate the expansion. This inequality holds in most experimental situations of interest [20].

As a result, I can write an elastic free energy in the case of an $n$-vector ferromagnet, with an average spin direction given by $\mathbf{n}$, as

$$F_{\text{el}} = \frac{1}{2}\int \mathrm{d}\mathbf{r}\; A(\nabla_i n_j)(\nabla_i n_j) \,, \tag{2.7}$$

where $A$ is the elastic constant that corresponds to the spin-wave stiffness in a magnet.

In the more general case of a liquid crystal, the spatial coordinates and the order parameter transform in the same way, which means that the elastic free energy need not be invariant under independent rotations of $\mathbf{n}$ and $\nabla$. This gives us in the most general case a fourth rank tensor, represented by $K_{ijkl}$, as the set of elastic constants for the problem:

$$F_{\mathrm{el}} = \frac{1}{2}\int \mathrm{d}\mathbf{r}\; K_{ijkl}(\nabla_i n_j)(\nabla_k n_l)\;, \tag{2.8}$$

Equation (2.8) is the most general possible expression for the Frank free energy. It must be invariant under the transformation $\mathbf{n} \to -\mathbf{n}$, $\mathbf{r} \to -\mathbf{r}$ and arbitrary rotations for a centrosymmetric system, as mentioned before. Furthermore, $\mathbf{n}$ is a unit vector ($\mathbf{n}^2 = 1$), which means that $\forall_{i,j}\; n_i \nabla_j n_i = 0$. These considerations imply that in a uniaxial system, $K_{ijkl}$ has three independent components, which are (1) *splay*, given by a non-vanishing $(\nabla \cdot \mathbf{n})^2$, as illustrated in figure 2.1(a), (2) *twist*, given by a non-zero $[\mathbf{n} \cdot (\nabla \times \mathbf{n})]^2$, as shown in figure 2.1(b), and (3) *bend*, given by a non-vanishing $[\mathbf{n} \times (\nabla \times \mathbf{n})]^2$, as seen in figure 2.1(c) [25]. That lets us rewrite the Frank free energy in the more concrete form,

$$F_{\mathrm{n}} = \frac{1}{2}\int \mathrm{d}\mathbf{r}\; \left\{K_1(\nabla \cdot \mathbf{n})^2 + K_2\left[\mathbf{n} \cdot (\nabla \times \mathbf{n})\right]^2 + K_3\left[\mathbf{n} \times (\nabla \times \mathbf{n})\right]^2\right\}\;. \tag{2.9}$$

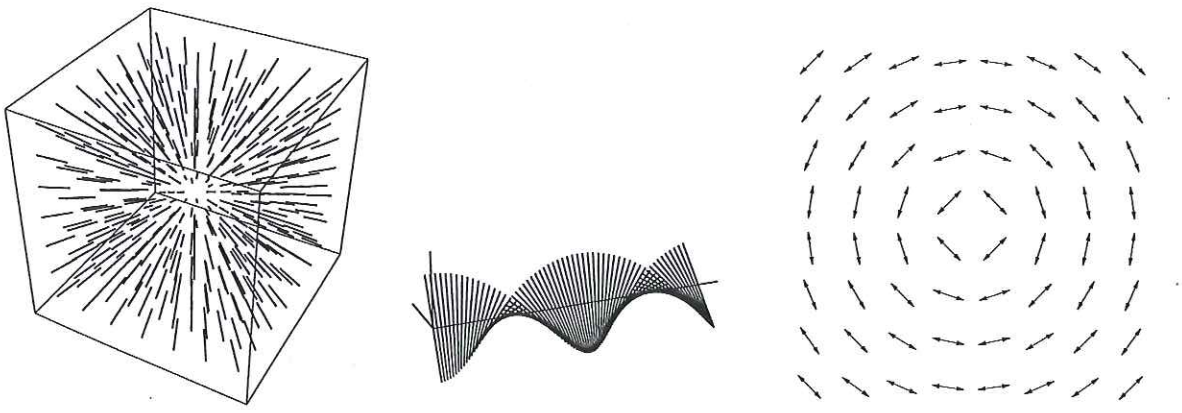

(a) Splay (b) Twist (c) Bend

Figure 2.1: Illustration of the three elastic deformation modes available to a liquid crystalline system, controlled by the elastic moduli $K_1$, $K_2$ and $K_3$, respectively.

However, if the individual molecules are chiral, then the material ceases to be centrosymmetric, which gives rise to a contribution to the free energy that is linear in the derivatives and proportional to $\mathbf{n} \cdot (\nabla \times \mathbf{n})$. I can complete the square in order to write

the free energy expression for a CLC in the form

$$F_{\mathrm{n}} = \frac{1}{2}\int \mathrm{d}\mathbf{r}\ \left\{K_1(\nabla\cdot\mathbf{n})^2 + K_2\left[\mathbf{n}\cdot(\nabla\times\mathbf{n}) + q_0\right]^2 + K_3\left[\mathbf{n}\times(\nabla\times\mathbf{n})\right]^2\right\}\ . \tag{2.10}$$

Clearly, since each term of equation (2.10) is positive definite, the free energy will be minimised when $\mathbf{n}\cdot(\nabla\times\mathbf{n}) = -q_0$. As can be seen in figure 2.1(b), a LC experiencing pure twist will wind periodically about a pitch axis. One choice of a director that minimises the free energy in equation (2.10) is

$$\mathbf{n} = \cos(q_0 z)\ \hat{x} + \sin(q_0 z)\ \hat{y}\ , \tag{2.11}$$

where $z$ is the pitch axis. In all further calculations, equation (2.11) will be assumed to be the ground state for an unperturbed CLC, as illustrated in figure 1.1.

## 2.5 External Fields

The equilibrium director field for a CLC is modified in a non-trivial way by an external electric or magnetic field. Since the optical properties of a CLC depend on the orientation of the mesogens, applying an external field should have a visible effect. Using the band structure techniques developed later in this thesis, I can predict these optical properties and compare them to previous experimental and numerical results [26]. Interestingly, this problem bears a strong resemblance to that of the application of strain to a cholesteric elastomer. Thus, results from this case can be applied, with some caveats, to the case of cholesteric elastomers. This issue will be discussed in detail in chapter 5.

There are, in general, both magnetic and electric anisotropies, designated by $\chi_a = \chi_{\parallel} - \chi_{\perp}$ and $\epsilon_a = \epsilon_{\parallel} - \epsilon_{\perp}$, respectively, that will cause the mesogens to align with an external field. Equation (2.10) giving the Frank free energy of the system will thus be augmented by the external fields' free energy contribution, given in references [27, 28] to be

$$F_{\mathrm{ext}} = -\int \mathrm{d}\mathbf{r}\ \left[\frac{1}{2}\chi_a(\mathbf{H}\cdot\mathbf{n})^2 + \frac{1}{8\pi}\epsilon_a(\mathbf{E}\cdot\mathbf{n})^2\right] \tag{2.12}$$

If I consider my cholesteric to be in a state of pure twist, so that the director field is given by equation (2.11), and experiences only an external magnetic field perpendicular to the pitch axis, then I can write a reduced expression for the free energy as

$$F_{\mathrm{cu}} = \frac{1}{2}\int \mathrm{d}\mathbf{r}\left\{K_2\left[\mathbf{n}\cdot(\nabla\times\mathbf{n}) + q_0\right]^2 - \chi_a(\mathbf{H}\cdot\mathbf{n})^2\right\}\ . \tag{2.13}$$

Given that the magnetic field points in the $xy$ plane, I can choose $\mathbf{H} = H\hat{x}$ without loss of generality. Then, I can calculate a free energy density, denoted by $f_{\rm cu}$, by integrating $F_{\rm cu}$ over one period and dividing by the volume to obtain

$$f_{\rm cu} = \frac{1}{2p_0}\int_0^{p_0} \mathrm{d}z \left\{ K_2 \left[ \left( \frac{\mathrm{d}\theta}{\mathrm{d}z} \right) - q_0 \right]^2 - \chi_a H^2 \cos^2\theta(z) \right\} , \tag{2.14}$$

where $p_0 = \pi/q_0$ is the pitch of the undistorted helix. Using the variational method, I can calculate that

$$\delta f_{\rm cu} \propto \int_0^{p_0} \mathrm{d}z \; \delta\theta \left[ \xi^2 \frac{\mathrm{d}^2\theta}{\mathrm{d}z^2} - \frac{1}{2}\sin 2\theta \right] , \tag{2.15}$$

where $\xi \equiv H^{-1}\sqrt{K_2/\chi_a}$. I choose to consider only real values of $\xi$, corresponding to $\chi_a > 0$, since otherwise the cholesteric will rotate so that its pitch axis points along the direction of the field, as expected for a negative dielectric anisotropy.

The quantity in brackets in equation (2.15) should vanish at a stationary point which corresponds to the minimum in free energy. Hence,

$$\xi^2 \frac{\mathrm{d}^2\theta}{\mathrm{d}z^2} = \sin\theta \;\; \cos\theta \; . \tag{2.16}$$

The first integral of this expression is given by

$$\xi^2 \left( \frac{\mathrm{d}\theta}{\mathrm{d}z} \right)^2 + \sin^2\theta = \frac{1}{k^2} = \text{const} , \tag{2.17}$$

where $k$ is a constant of integration. Physically, this solution describes a coarsening of the helical structure which increases the fraction of favourable alignments between mesogens and the field, while preserving a memory of the cholesteric structure, as illustrated figures 2.2 and 2.3.

The coarsening requires the creation of twist walls, regions where the director twist rapidly when making the transition between two regions of favourable alignment. Intuitively, in the limit of extremely strong fields, one would expect the twist walls to be unstable, and give way to total alignment, i.e., a regular nematic phase.

The field strength at which complete unwinding occurs can be found by calculating the relative free energy density of the distorted cholesteric and nematic phases, which I

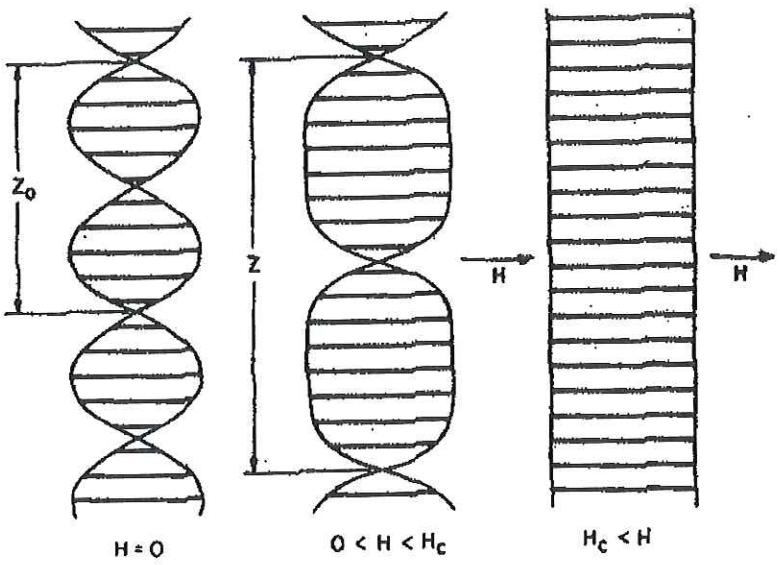


Figure 2.2: Untwisting of a cholesteric helix in an external field (adapted from reference [29]).

designate as $f_w$:

$$f_w \sim \frac{1}{2p_0}\int_0^{p_0} \mathrm{d}z \left\{ K_2 \left[ \left( \frac{\mathrm{d}\theta}{\mathrm{d}z} - q_0 \right)^2 - q_0^2 \right] + \chi_a H^2 \sin^2\theta \right\} . \tag{2.18}$$

I can rewrite this expression with a reduced free energy $f'_w$ given by

$$f'_w \equiv \frac{2p_0}{\chi_a H^2} f_w \sim \int_0^{p_0} \mathrm{d}z \left\{ \xi^2 \left[ \left( \frac{\mathrm{d}\theta}{\mathrm{d}z} \right)^2 - 2q_0 \left( \frac{\mathrm{d}\theta}{\mathrm{d}z} \right) \right] + \sin^2\theta \right\} . \tag{2.19}$$

The first integral of the ODE describing the coarsening of the helix, equation (2.16), tells us the first and third terms are equal. I can thus rewrite my expression as

$$f'_w \sim 2\xi^2 \int_0^{p_0} \mathrm{d}z \left[ \left( \frac{\mathrm{d}\theta}{\mathrm{d}z} \right)^2 - 2q_0 \left( \frac{\mathrm{d}\theta}{\mathrm{d}z} \right) \right] . \tag{2.20}$$

Expressing equation (2.20) in terms of $\theta$ gives us

$$f'_w \sim 2\xi^2 \int_0^{\pi} \mathrm{d}\theta \left( \left| \frac{\mathrm{d}\theta}{\mathrm{d}z} \right| - q_0 \right) , \tag{2.21}$$

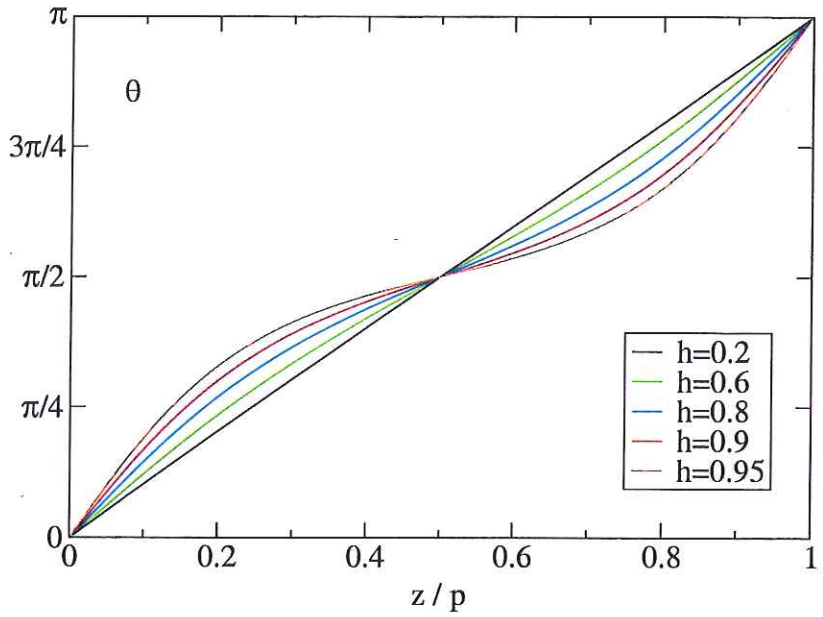


Figure 2.3: Angular orientation of the director, $\theta$, versus the reduced position $\tilde{z} = z/p$ for several values of the reduced field $h = H/H_c$.

or

$$f_w' \sim 2\xi \int_0^{\pi} \mathrm{d}\theta \ (\sin\theta - \xi q_0) \ . \tag{2.22}$$

Equation (2.22) says that $f_w \propto 2 - \pi q_0 \xi$, which suggests that a cross-over between a negative $f_w$, corresponding to a cholesteric phase, and a positive $f_w$, corresponding to an untwisted nematic phase, takes place at a critical field $\xi_c = 2/\pi q_0$. The critical $\xi_c$ corresponds to a critical field $H_c = (\pi q_0/2)\sqrt{K_2/\chi_a}$. Increasing $H$ is accompanied by a lengthening of the pitch, which diverges as $H \to H_c$. I can calculate the pitch length at a given $H$ by integrating $\left(\frac{\mathrm{d}\theta}{\mathrm{d}z}\right)^{-1}$ over one period, which gives me a new pitch $p = 2\xi k K(k^2)$, where $K(k^2)$ is the complete elliptic integral of the first kind [30], and $k$ is the constant of integration from equation (2.17). It is easy to show that $k = \frac{\pi}{2}\frac{H}{H_c}$. The new pitch will be greater than the pitch at zero field, and will diverge as $H \to H_c$, as required. See figure 2.4.

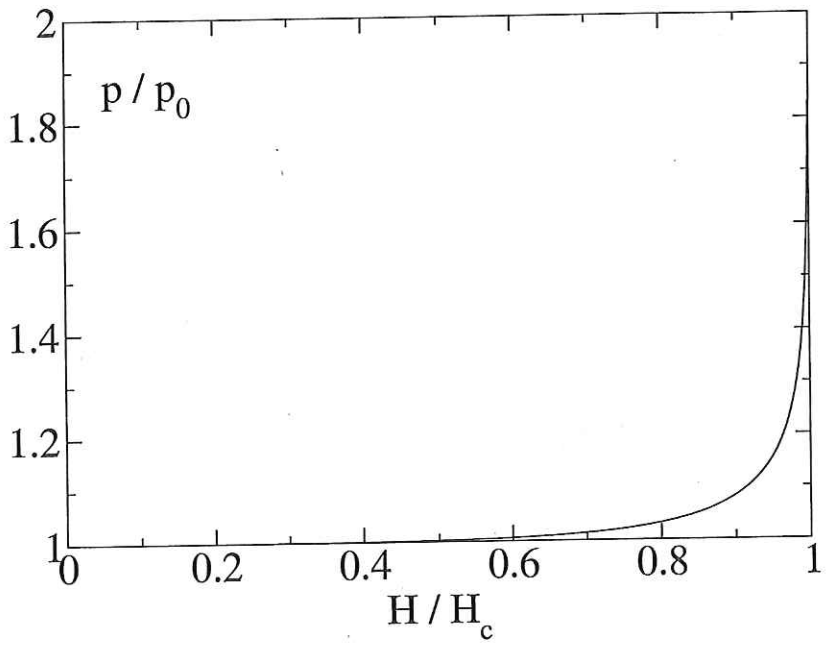


Figure 2.4: A plot of the relative pitch $p/p_0$ as a function of the magnetic field as a fraction of the critical field. Notice the rapid divergence of the pitch as $H \to H_c$.

# Chapter 3

# Nematic Rubber Theory

## 3.1 Isotropic Rubbers

In the simplest models of rubbers, such as the Flory model, one assumes that they consist of non-interacting polymer chains anchored by cross-links. The polymer chains execute a random walk in space, independent of other chains, in the so-called "phantom chain" approximation. An ensemble of polymer chains with $N$ subunits of length $a$ will have a Gaussian distribution of chain lengths $R$, given by $\mathcal{P}(R) \sim e^{-R^2/2Na^2}$ in one dimension. This distribution has a vanishing first moment $\langle R \rangle = 0$ and a non-vanishing second moment $\langle R^2 \rangle = Na^2$. In the isotropic 3-D case, these results may be generalised to vectors $\mathbf{R}$ whose second moments are given by $\langle R_i R_j \rangle = \frac{1}{3} Na^2 \delta_{ij}$ (which recovers the result $\langle \mathbf{R}^2 \rangle = Na^2$). Thus, $\mathcal{P}(\mathbf{R}) \sim e^{-3\mathbf{R}^2/2Na^2}$.

The macroscopic deformation which an elastomeric network experiences is given by a second-rank tensor, referred to as the deformation tensor $\underline{\underline{\lambda}}$. The strain is given by the symmetric part of the difference of the deformation tensor and the unit tensor, i.e., $\underline{\underline{e}} = \hat{\mathcal{S}}\left(\underline{\underline{\lambda}} - \underline{\underline{\delta}}\right)$, where $\hat{\mathcal{S}}$ is a symmetrisation operator defined so that $\hat{\mathcal{S}}\,\underline{\underline{A}} = \frac{1}{2}\left(\underline{\underline{A}} + \underline{\underline{A}}^{\dagger}\right)$. Within the assumption of affine network deformation, the average positions of the cross-links anchoring the ends of the polymers follow the macroscopic strain, i.e., the end-to-end distance vector $\mathbf{R} \to \mathbf{R}' = \underline{\underline{\lambda}} \cdot \mathbf{R}$ for all chains. As a result, the expression for the entropy of a single, deformed chain is expected to be [31]

$$S(\mathbf{R}) = k_B \left[ N \ln 2 - \frac{3}{2} \frac{(\underline{\underline{\lambda}} \cdot \mathbf{R})^2}{Na^2} \right] . \tag{3.1}$$

Given that no bonds are broken or formed, and neglecting intermolecular (van der Waals) interactions, the free energy $F$ is given simply by $F = F_0 - TS$. Since $F_0$ is arbitrary, it may be set to zero for the remainder of this derivation. Substituting in equation (3.1), I

obtain the following expression for the free energy of a single chain:

$$F_{\underline{\underline{\lambda}}}(\mathbf{R}) = \frac{3}{2}k_BT\frac{(\underline{\underline{\lambda}}\cdot\mathbf{R})^2}{Na^2}\ . \tag{3.2}$$

The total free energy of the system will be the energy of each individual chain, averaged over the distribution of $\mathbf{R}$ and multiplied by the number density of chains $\nu$. In quenched averaging, I assume that the probability of finding a span $\mathbf{R}'$ after deformation is that of finding the $\mathbf{R}$ at formation from which it evolved. Thus, I average $F(\mathbf{R}')$ over my initial distribution $\mathcal{P}(\mathbf{R})$ to obtain the free energy density, given explicitly by

$$\langle F\rangle = \frac{3}{2}\frac{\nu k_BT}{Na^2}\frac{\int \mathrm{d}\mathbf{R}\ (\underline{\underline{\lambda}}\cdot\mathbf{R})^2 e^{-3\mathbf{R}^2/2Na^2}}{\int \mathrm{d}\mathbf{R}\ e^{-3\mathbf{R}^2/2Na^2}}\ . \tag{3.3}$$

I can rewrite this in the form

$$\langle F\rangle = \frac{3}{2}\frac{\nu k_BT}{Na^2}\lambda_{ai}\lambda_{aj}\frac{\int \mathrm{d}\mathbf{R}\ R_iR_j e^{-3\mathbf{R}^2/2Na^2}}{\int \mathrm{d}\mathbf{R}\ e^{-3\mathbf{R}^2/2Na^2}}\ . \tag{3.4}$$

Since the ratios of integrals is simply $\langle R_iR_j\rangle = \frac{1}{3}Na^2\delta_{ij}$, I can immediately deduce that

$$\langle F\rangle = \frac{1}{2}\nu k_BT\ \mathrm{Tr}\left(\underline{\underline{\lambda}}^T\cdot\underline{\underline{\lambda}}\right)\ . \tag{3.5}$$

I note that this solution is rotationally invariant and independent of the details of the distribution of cross-links. In the simplest case, I assume that the stretching takes place along one of the principal axes of the system, and has a magnitude $\lambda$. Physically, the large value of the bulk modulus of a rubber, compared to its shear modulus, ensures that it deforms at constant volume to one part in $10^4$. Then by symmetry, an isotropic rubber stretched by $\lambda$ in one direction should shrink by a factor of $1/\sqrt{\lambda}$ in the other two directions – see figure 3.1. Hence,

$$\underline{\underline{\lambda}} = \begin{pmatrix} \lambda & 0 & 0 \\ 0 & \frac{1}{\sqrt{\lambda}} & 0 \\ 0 & 0 & \frac{1}{\sqrt{\lambda}} \end{pmatrix}\ , \tag{3.6}$$

which gives the simple result that

$$\langle F\rangle = \frac{1}{2}\nu k_BT\left(\lambda^2 + \frac{2}{\lambda}\right)\ . \tag{3.7}$$

Equation (3.5) represents one of the major results of the theory of elastomers. Starting from the total free energy expression, one can easily calculate all other thermodynamic

quantities of interest, such as elastic response [32].

## 3.2 Nematic Rubbers

In a nematic rubber, the isotropy of a normal rubber is broken by the local nematic ordering. In the case of a uniaxial nematic, which has been discussed previously, it is reasonable to expect by analogy with other quantities that the step size for polymers is different depending on whether I move along or perpendicular to the local nematic ordering. I thus generalise my isotropic step size $a$ into two components $a_\parallel$ in the direction of the nematic order, and $a_\perp$ in either direction perpendicular to the nematic order. As a result, the previously isotropic function $\langle R_i R_j \rangle = \frac{1}{3} N a^2 \delta_{ij}$ becomes $\langle R_i R_j \rangle = \frac{1}{3} a_{ij} \mathcal{L}$ , where

$$a_{ij} = (a_\parallel - a_\perp) n_i n_j + a_\perp \delta_{ij} \, , \tag{3.8}$$

and $\mathcal{L}$ is the total contour length of the chain between cross links (given by $aN$). For a freely-jointed chain polymer, I can calculate $\underline{\underline{a}}$ in terms of the nematic order parameter, and obtain the result $\underline{\underline{a}} = a(\underline{\underline{\delta}} + 2\underline{\underline{Q}})$ The probability distribution for the end-to-end vector, previously given by $\mathcal{P}(\mathbf{R}) \sim \exp\left[-\frac{3}{2a\mathcal{L}}\mathbf{R}^2\right]$, generalises to $\mathcal{P}(\mathbf{R}) \sim \exp\left[-\frac{3}{2\mathcal{L}}\mathbf{R} \cdot \underline{\underline{a}}^{-1} \cdot \mathbf{R}\right]$. This allows me to generalise the Helmholtz free energy expression for an individual chain, equation (3.2), to

$$F_{\underline{\underline{\lambda}}}(\mathbf{R}) = \frac{3}{2} \frac{k_B T}{\mathcal{L}} (\underline{\underline{\lambda}} \cdot \mathbf{R}) \cdot \underline{\underline{a}}^{-1} \cdot (\underline{\underline{\lambda}} \cdot \mathbf{R}) \, . \tag{3.9}$$

In order to find the free energy of a macroscopic rubber under strain, I perform a quenched average of the stretched chains' energy over the initial distribution, $\mathcal{P}_0(\mathbf{R})$, of end-to-end vectors, present at formation, so that

$$\langle F \rangle = \frac{3}{2} \frac{\nu k_B T}{\mathcal{L}} \frac{\int \mathrm{d}\mathbf{R} \, \left[(\underline{\underline{\lambda}} \cdot \mathbf{R}) \cdot \underline{\underline{a}}^{-1} \cdot (\underline{\underline{\lambda}} \cdot \mathbf{R})\right] e^{-3\mathbf{R} \cdot \underline{\underline{a}}_0^{-1} \cdot \mathbf{R}/2\mathcal{L}}}{\int \mathrm{d}\mathbf{R} \, e^{-3\mathbf{R} \cdot \underline{\underline{a}}_0^{-1} \cdot \mathbf{R}/2\mathcal{L}}} \, . \tag{3.10}$$

Since again, the average correlation $\langle \mathbf{RR} \rangle = \frac{1}{3} \underline{\underline{a}}_0 \mathcal{L}$, the result can be shown to be

$$\langle F \rangle = \frac{1}{2} \nu k_B T \, \mathrm{Tr}\left[\underline{\underline{a}}_0 \cdot \left(\underline{\underline{\lambda}}^T \cdot \underline{\underline{a}}^{-1} \cdot \underline{\underline{\lambda}}\right)\right] \, . \tag{3.11}$$

Nematic rubbers display spontaneous thermal expansion of an extreme form [33]. If nematics are cooled below the nematic-isotropic transition temperature, there is an onset of order, and in light of this discussion, a corresponding transition from the initially isotropic random walk to an anisotropic random walk. I can estimate the magnitude

of this deformation by substituting the appropriate $\underline{\underline{a}}_0 = a\underline{\underline{\delta}}$ and the anisotropic $\underline{\underline{a}}$ from equation (3.8) into equation (3.11) to obtain

$$\langle F \rangle = \frac{1}{2}\nu k_B T \left[ \frac{a}{a_\parallel}\lambda^2 + 2\frac{a}{a_\perp}\frac{1}{\lambda} \right] . \tag{3.12}$$

Minimisation of $\langle F \rangle$ with respect to $\lambda$ yields a spontaneous deformation of $\lambda_s = \sqrt[3]{a_\parallel/a_\perp}$. The parameter $r$ is defined to be the ratio $a_\parallel/a_\perp$. This quantity is experimentally accessible through the measurement of the magnitude of $\lambda_s$, and is important because it sets the scale of anisotropy in the network, making it an important measure in what will follow. For nematic rubbers of interest, $r$ can range anywhere from 1.1 to 64, which corresponds to spontaneous deformations $\lambda_s$ between 1.03 and 4.

Another novel phenomenon observed in nematic rubbers is soft elasticity [34]. Following [35], I can guess that strains of the following form will cost no energy:

$$\underline{\underline{\lambda}} = \underline{\underline{a}}^{1/2} \cdot \underline{\underline{\mathcal{R}}} \cdot \underline{\underline{a}}_0^{-1/2} , \tag{3.13}$$

where $\underline{\underline{\mathcal{R}}}$ is an arbitrary rotation (the SU(3) group in three dimensions). This guess can be verified by substituting equation (3.13) into equation (3.11) to obtain

$$\langle F \rangle = \frac{1}{2}\nu k_B T \, \mathrm{Tr}\left[ \underline{\underline{a}}_0 \cdot \left( \underline{\underline{a}}_0^{-1/2} \cdot \underline{\underline{\mathcal{R}}}^T \cdot \underline{\underline{a}}^{1/2} \cdot \underline{\underline{a}}^{-1} \cdot \underline{\underline{a}}^{1/2} \cdot \underline{\underline{\mathcal{R}}} \cdot \underline{\underline{a}}_0^{-1/2} \right) \right] . \tag{3.14}$$

Since $\underline{\underline{\mathcal{R}}}^T = \underline{\underline{\mathcal{R}}}^{-1}$ by definition, the result that $\langle F \rangle = \frac{3}{2}\nu k_B T$ for all $\underline{\underline{\mathcal{R}}}$ is obtained. In other words, strains of the form given by equation (3.13) do not cause the free energy to increase above its value in the fully relaxed state. Thus, it is expected that strains of this type will produce almost no stress. This has been observed experimentally to a good approximation in some nematic elastomers [34].

An concrete example of soft elasticity may help illustrate how it differs from conventional elasticity. If extension occurs along the $x$-axis so that $\mathbf{n}_0 = \hat{y}$ becomes $\mathbf{n} = \hat{x}$, the appropriate $\underline{\underline{a}}$ and $\underline{\underline{a}}_0$ can be found by substitution into equation (3.8). The equation for the soft elastic response deformation tensor, equation (3.13), yields the result, for $\underline{\underline{\mathcal{R}}} = \underline{\underline{\delta}}$, that

$$\underline{\underline{\lambda}} = \begin{pmatrix} \sqrt{a_\parallel/a_\perp} & 0 & 0 \\ 0 & \sqrt{a_\perp/a_\parallel} & 0 \\ 0 & 0 & 1 \end{pmatrix} . \tag{3.15}$$

In sharp contrast to the classical response, given by equation (3.6), a deformation of $\lambda$ orthogonal to the original nematic field induces a contraction of $\lambda^{-1}$ along the direction

the director originally pointed toward, and no contraction in the third direction. See figure 3.1 for a graphical comparison.

## 3.3 Cholesteric Rubbers

A more difficult question concerns the prediction of what happens to a cholesteric rubber under deformation. The nematic order breaks the symmetry of the rubber in the direction of the pitch axis, which I assume without loss of generality points along $z$. For an extension of magnitude $\lambda$ in the $x$ direction, in the plane of the nematic order, I have the deformation tensor,

$$\underline{\underline{\lambda}} = \begin{pmatrix} \lambda & 0 & 0 \\ 0 & \lambda_{yy} & 0 \\ 0 & 0 & \frac{1}{\lambda\lambda_{yy}} \end{pmatrix} . \tag{3.16}$$

Clearly, the volume does not change (i.e., $\det \underline{\underline{\lambda}} = 1$); however, contractions in the $y$ and $z$ directions will be different in general, unlike in an isotropic rubber, as is evident from equation (3.6). I have suppressed shears (off-diagonal elements of $\underline{\underline{\lambda}}$), since in this geometry, they will cost a large energy that scales linearly with the sample size – in the thermodynamic limit, they are forbidden [23]. For a cholesteric rubber, then, one may substitute equation (2.11) for the CLC director into equation (3.8) to obtain

$$\underline{\underline{a}}_0 = a_\perp \left[ \underline{\underline{\delta}} + (r-1) \begin{pmatrix} \cos^2\phi_0 & \cos\phi_0 \sin\phi_0 & 0 \\ \cos\phi_0 \sin\phi_0 & \sin^2\phi_0 & 0 \\ 0 & 0 & 0 \end{pmatrix} \right] , \tag{3.17}$$

and similarly, that

$$\underline{\underline{a}}^{-1} = \frac{1}{a_\perp} \left[ \underline{\underline{\delta}} + \frac{1-r}{r} \begin{pmatrix} \cos^2\phi & \cos\phi \sin\phi & 0 \\ \cos\phi \sin\phi & \sin^2\phi & 0 \\ 0 & 0 & 0 \end{pmatrix} \right] . \tag{3.18}$$

In order to calculate the free energy, I can substitute equations (3.16-3.18) into my canonical free energy expression, equation (3.11) to obtain an expression for the free

energy, $\langle F \rangle = \langle F(\lambda, \lambda_{yy}, r, \phi, \phi_0) \rangle$. I write the raw local free energy expression as

$$\langle F \rangle = \frac{1}{2}\nu k_B T \left\{ \frac{1}{\lambda^2 \lambda_{yy}^2} + \lambda^2 \left[ 1 - \frac{r-1}{r} \cos^2 \phi \right] \left[ 1 + (r-1)\cos^2 \phi_0 \right] \right.$$
$$\left. -2\lambda\lambda_{yy} \frac{(r-1)^2}{r} \cos\phi \cos\phi_0 \sin\phi \sin\phi_0 + \lambda_{yy}^2 \left[ 1 + \frac{1-r}{r} \sin^2 \phi \right] \left[ 1 + (r-1)\sin^2 \phi_0 \right] \right\} . \tag{3.19}$$

This expression can be simplified to the following form, given in [23]:

$$\langle F \rangle = \frac{1}{2}\nu k_B T \left\{ \lambda^2 + \lambda_{yy}^2 + \frac{1}{\lambda^2 \lambda_{yy}^2} + \frac{r-1}{r} \left[ \lambda^2 \left( r\cos^2 \phi_0 \sin^2 \phi - \sin^2 \phi_0 \cos^2 \phi \right) \right. \right.$$
$$\left. \left. +\lambda_{yy}^2 \left( r\sin^2 \phi_0 \cos^2 \phi - \cos^2 \phi_0 \sin^2 \phi \right) - 2(r-1)\lambda\lambda_{yy} \cos\phi \cos\phi_0 \sin\phi \sin\phi_0 \right] \right\} . \tag{3.20}$$

In order to calculate the local director orientation, I can look for critical values of equation (3.20) by setting $\partial \langle F \rangle / \partial\phi = 0$. I obtain the result, given in [23], that

$$\tan 2\phi = \frac{2(r-1)\lambda\lambda_{yy} \sin 2\phi_0}{(r-1)\left(\lambda^2 + \lambda_{yy}^2\right)\cos 2\phi_0 + (r+1)\left(\lambda^2 - \lambda_{yy}^2\right)} . \tag{3.21}$$

I now discuss some results based on this work that I have derived independently in the course of my research and which are currently unpublished. I can determine whether the values given by equation (3.21) are stable by calculating $\partial^2 \langle F \rangle / \partial\phi^2$ from equation (3.20) and backsubstituting equation (3.21) into the expression for the second derivative. I obtain the result that

$$\frac{\partial^2 \langle F \rangle}{\partial\phi^2} = \frac{1}{4r\lambda\lambda_{yy}} \nu k_B T \left\{ \left[ (r+1)\left(\lambda^2 - \lambda_{yy}^2\right) + (r-1)\left(\lambda^2 + \lambda_{yy}^2\right)\cos 2\phi_0 \right]^2 \right.$$
$$\left. +4(r-1)^2 \lambda^2 \lambda_{yy}^2 \sin^2 2\phi_0 \right\} \left( \frac{\sin 2\phi}{\sin 2\phi_0} \right) . \tag{3.22}$$

Since the quantities in braces are positive definite, the sign of $\partial^2 \langle F \rangle / \partial\phi^2$ will be given by the sign of $\sin 2\phi / \sin 2\phi_0$. Thus, when $\sin 2\phi$ and $\sin 2\phi_0$ are of the same sign, the second derivative will be positive, corresponding to a local minimum in free energy. One can then use equation (3.21), trigonometric identities combined with this stability analysis to obtain $\cos 2\phi$ and $\sin 2\phi$, which are thus given by

$$\sin 2\phi = \frac{(r-1)\lambda\lambda_{yy} \sin 2\phi_0}{\sqrt{a_1^2 - 4r\lambda^2\lambda_{yy}^2}}, \tag{3.23}$$

and

$$\cos 2\phi = -\frac{\lambda_{yy}^2 - r\lambda^2 + (r-1)\left(\lambda^2 + \lambda_{yy}^2\right)\sin^2\phi_0}{\sqrt{a_1^2 - 4r\lambda^2\lambda_{yy}^2}}\,, \tag{3.24}$$

where $a_1 = r\lambda^2 + \lambda_{yy}^2 - (r-1)\left(\lambda^2 - \lambda_{yy}^2\right)\sin^2\phi_0$. I can substitute these values back into equation (3.20), to obtain $\langle F\rangle = \langle F(\lambda, \lambda_{yy}, r, \phi_0)\rangle$. I then coarse-grain my free energy expression over one complete turn of the helix, and define the coarse-grained free energy density $\langle F'\rangle$ such that $\langle F'(\lambda, \lambda_{yy}, r)\rangle = \int_0^\pi \mathrm{d}\phi_0\ \langle F(\lambda, \lambda_{yy}, r, \phi_0)\rangle$. Given a fixed value for $\lambda$ and $r$, I can find the minimum-energy value of $\lambda_{yy}$ by setting $\partial\langle F'\rangle/\partial\lambda_{yy} = 0$. If we assume that $\lambda_{yy}$ is a power law in terms of $\lambda$ in the limit of small strains ($\lambda \to 1$), then we can use a perturbation analysis to obtain the correct exponent. In the first step, the energy minimisation condition is written explicitly as

$$\begin{aligned} 0 = {} & \pi - \frac{\pi}{\lambda^2\lambda_{yy}^4} + \frac{\pi}{4}\frac{(r-1)^2}{r} \\ & + \frac{r-1}{r}\int_0^{\pi/2} \mathrm{d}\phi_0 \left[\left(r\sin^2\phi_0 + \cos^2\phi_0\right)\cos 2\phi - \frac{r-1}{2}\frac{\lambda}{\lambda_{yy}}\sin 2\phi_0 \sin 2\phi\right]\,. \end{aligned} \tag{3.25}$$

Next, substitution of the appropriate expressions for $\sin 2\phi$ and $\cos 2\phi$, equations (3.23) and (3.24), yields

$$\frac{\pi}{4}\frac{(r+1)^2}{r} - \frac{\pi}{\lambda^2\lambda_{yy}^4} - \frac{r-1}{r}\int_0^{\pi/2} \mathrm{d}\phi_0 \left\{\frac{a_1\left[1 + (r-1)\sin^2\phi_0\right] - 2r\lambda^2}{\sqrt{a_1^2 - 4r\lambda^2\lambda_{yy}^2}}\right\} = 0\,. \tag{3.26}$$

Equation (3.26) may be written in a simplified form such that

$$\frac{\pi}{4}\frac{(r+1)^2}{r} - \frac{\pi}{\beta^2\lambda^6} - \frac{r-1}{r}\int_0^{\pi/2} \mathrm{d}\phi_0 \left\{\frac{a_1'\left[1 + (r-1)\sin^2\phi_0\right] - 2r}{\sqrt{a_1'^2 - 4r\beta}}\right\} = 0\,, \tag{3.27}$$

where $a_1' = a_1/\lambda^2$ and $\beta = \lambda_{yy}^2/\lambda^2$. Now, since $\lambda = 1 + e$, where $e \ll 1$, and $\beta = \lambda^{-\varpi} \approx 1 - \varpi e$ by assumption, they can be substituted into equation (3.27) to produce an expression to the first order in $e$, namely,

$$\pi\left[\frac{(r+1)^2}{4r} - 1 + (6 - 2\varpi)\,e\right] - \frac{\pi}{4r}\left[(r-1)^2 - r\varpi e\right] = 0\,. \tag{3.28}$$

The left hand side vanishes when $\varpi = 24/7$ (to the first order), which, given the definitions of $\beta$ and $\varpi$, implies that $\lambda_{yy} = \lambda^{-5/7}$. Of course, this scaling is only valid for small $e$. There is a critical strain, denoted by $e_c$, and an accompanying critical deformation

$\lambda_c = 1 + e_c$, at which the twist walls created by the strain become thermodynamically unfavourable. At that point the director loses its cholesteric ordering and oscillates back and forth around $\phi = 0$. There will also be a cross-over from the scaling behaviour $\lambda_{yy} \sim \lambda^{-5/7}$ for small strain, to the classical isotropic response, $\lambda_{yy} \sim \lambda^{-1/2}$, for large strain. Mathematically, since the divergence of a tangent function signifies crossing between branch cuts, a $\tan 2\phi$ which is finite for all $\phi_0$ in interpreted to oscillate within just one branch cut, conventionally chosen to be the interval $(-\pi/2, \pi/2]$. The $\tan 2\phi$ will only diverge if the denominator crosses zero, so the critical strain corresponds to the point at which the denominator is guaranteed to be greater than or equal to zero. Thus, the condition, derived from equation (3.21), that

$$\forall_{\phi_0} \quad (r-1)\left(\lambda^2 + \lambda_{yy}^2\right)\cos 2\phi_0 + (r+1)\left(\lambda^2 - \lambda_{yy}^2\right) \geq 0 \tag{3.29}$$

Since $\cos 2\phi_0$ is bounded between $\pm 1$, equation (3.29) is equivalent to the requirement that

$$(r+1)\left(\lambda^2 - \lambda_{yy}^2\right) \geq (r-1)\left(\lambda^2 + \lambda_{yy}^2\right) \ . \tag{3.30}$$

If it is assumed that $e \ll 1$, and that $\lambda_{yy} \sim \lambda^{-\kappa}$, then the following result may be obtained:

$$(r+1)(1+\kappa)e \geq (r-1)\left[1 + (1-\kappa)e\right] \ . \tag{3.31}$$

Thus, the

$$e_c \approx \frac{r-1}{(r+1)(\kappa+1) + (r-1)(\kappa-1)} \tag{3.32}$$

Expanding the expression for $e_c$ to the first order in $r-1$ yields the result, $e_c = (r-1)/\left[2(1+\kappa)\right]$. Inspection of figure 3.1 suggests that $\kappa \approx 3/4$, a value close to the initial $\kappa = 5/7$ which is strictly correct only for $\lambda \to 1$. As a result, it can easily be shown that $\lambda_c \approx r^{2/7}$, to the first order.

Although obtaining an exact analytic solution is infeasible, I can find the critical values for $\langle F' \rangle$ (with respect to $\lambda_{yy}$) numerically, as shown in figure 3.1. I can confirm that, for parameter values of interest (e.g., $r = 1.9$, $1 \leq \lambda \leq 1.4$), a minimum-energy state occurs at values of $\lambda_{yy} \approx \lambda^{-3/4}$ for $e < e_c$. There is also evidently a cross-over to the classical scaling $\lambda_{yy} \approx \lambda^{-1/2}$, for $e > e_c$.

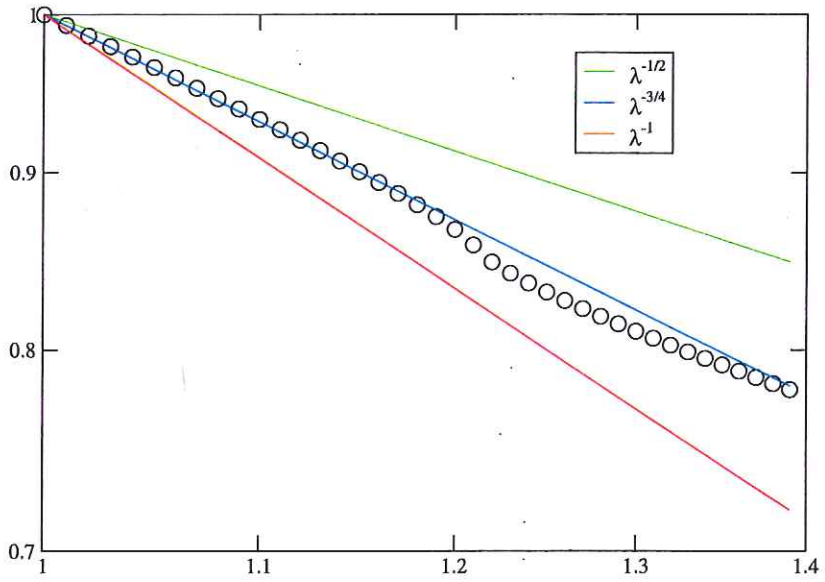


Figure 3.1: Numerical calculation of the contraction of a cholesteric elastomer $\lambda_{yy}$ as a function of the applied uniaxial strain $\lambda$ for $r = 1.9$ ($\lambda_c \approx 1.19$).

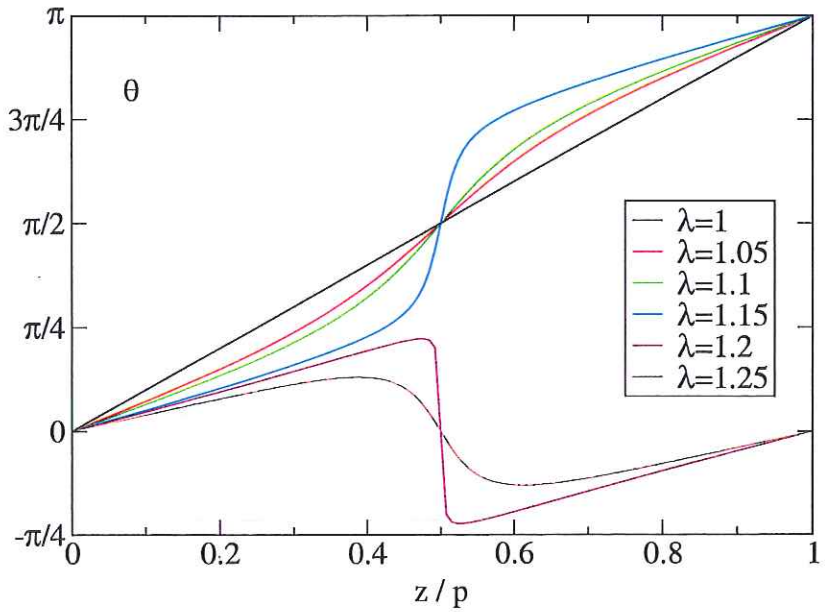


Figure 3.2: Dependence of the orientation of the director on distance along pitch axis for helices subjected to several different $x$-strains of magnitude $\lambda$. Notice the qualitative change in behaviour as $\lambda$ crosses through $\lambda_c \approx 1.19$.

# Chapter 4

# CLC Optics: de Vries' Approach

In this chapter, I discuss de Vries' approach to understanding the optical properties of an ideal cholesteric medium, described by the director field given in equation (2.11). De Vries starts with Maxwell's equations written in the form of a wave equation, and transforms into a rotating coordinate system. He is able to solve the optical properties exactly for a perfect helix. However, when there are deviations from a uniform advancement of the angle of the director, de Vries' approach fails to give an analytical result. An approach based on a different formalism is thus called for, and discussed in the next chapter. Nonetheless, de Vries' approach is important as a baseline for understanding the optics of CLC's, and is consequently reviewed here in detail.

The solution begins with Maxwell's equations, exact for linear media, which are given by:

$$\nabla \cdot \mathbf{D} = 4\pi\rho \tag{4.1}$$

$$\nabla \cdot \mathbf{B} = 0 \tag{4.2}$$

$$\nabla \times \mathbf{E} = -\frac{1}{c}\frac{\partial \mathbf{B}}{\partial t} \tag{4.3}$$

$$\nabla \times \mathbf{H} = \frac{4\pi}{c}\mathbf{J} + \frac{1}{c}\frac{\partial \mathbf{D}}{\partial t} \tag{4.4}$$

Assuming that there are no free charges or currents in the system, I can reduce equations (4.1) and (4.4) to:

$$\nabla \cdot \mathbf{D} = 0 \tag{4.5}$$

$$\nabla \times \mathbf{H} = \frac{1}{c}\frac{\partial \mathbf{D}}{\partial t} \tag{4.6}$$

Given that the auxiliary equation $\mathbf{D} = \underline{\underline{\epsilon}}\mathbf{E}$ is time-independent, I can rewrite equation 4.6 as $\underline{\underline{\epsilon}}^{-1}(\mathbf{r})(\nabla \times \mathbf{H}) = \frac{1}{c}\frac{\partial \mathbf{E}}{\partial t}$. Then, I apply the curl operator to obtain $\nabla \times$

$\left[\underline{\underline{\epsilon}}^{-1}(\mathbf{r})(\nabla \times \mathbf{H})\right] = \frac{1}{c}\frac{\partial}{\partial t}(\nabla \times \mathbf{E})$. If I substitute my expression for $\nabla \times \mathbf{E}$, equation 4.3, and assume that my magnetic permeability is homogeneous throughout my medium, I obtain

$$\nabla \times \left[\underline{\underline{\epsilon}}^{-1}(\mathbf{r})(\nabla \times \mathbf{H})\right] = -\frac{1}{c^2}\frac{\partial^2 \mathbf{H}}{\partial t^2} \,. \tag{4.7}$$

This result is in the form of a wave equation, as expected. Assuming each wave has one, well-defined frequency, the magnetic field may be rewritten as $\mathbf{H}(\mathbf{r}, t) = \mathbf{H}(\mathbf{r})\, e^{i\omega t}$. This gives rise to the eigen-like expression,

$$\nabla \times \left[\underline{\underline{\epsilon}}^{-1}(\mathbf{r})(\nabla \times \mathbf{H})\right] = \frac{\omega^2}{c^2}\mathbf{H} \,, \tag{4.8}$$

which may be used as the basis for calculating the magnetic field throughout the medium.

## 4.1 Ideal Helix, Normal Incidence

I now aim to reformulate de Vries' results using modern notation and in a slightly more general fashion.

For a plane-wave propagating along the $z$-axis (normal incidence), Maxwell's equations (4.1-4.4) may be combined in a slightly different way into the simple wave equation,

$$\left(\frac{\omega}{c}\right)^2 \mathbf{D} = -\frac{\partial^2 \mathbf{E}}{\partial z^2} \,. \tag{4.9}$$

By symmetry, $\mathbf{D}$ must be the same for any $(x, y)$ pair. Because of the transversality constraint of equation (4.5), $\mathbf{D}$ must exist wholly in the $xy$ plane. Then, by equation (4.9), $\mathbf{E} \cdot \hat{z} = Az + B$. By periodicity, $A = 0$, and by boundary conditions (no free charges on the surface), $B = 0$, which means that $\mathbf{E}$ also points wholly in the $xy$ plane.

I expect most cholesteric liquid crystals to be locally uniaxial with one optical axis along the director field $\mathbf{n}(\mathbf{r})$. Of course, in the most general case, a cholesteric liquid crystal will be biaxial, but theoretical considerations [20] and studies of oblique incidence by Berreman and Scheffer in the 1970s [36] strongly suggest that $\epsilon_3 = \epsilon_\perp$ to one part in $(q_0 a)^2 \approx 10^{-4}$, where $a$ is the molecular dimension of liquid crystal subunits.

As a result, I can write the dielectric tensor in the form, $\epsilon_{ij} = (\epsilon_\parallel - \epsilon_\perp) n_i n_j + \epsilon_\perp \delta_{ij}$, where $\epsilon_\parallel$ is the dielectric constant along the long axis of the nematic mesogen, and $\epsilon_\perp$ is the dielectric constant in any direction perpendicular to the mesogenic axis. Usually I define for convenience the quantity $\epsilon_a = \epsilon_\parallel - \epsilon_\perp$ so that I can write

$$\epsilon_{ij} = \epsilon_a n_i n_j + \epsilon_\perp \delta_{ij} \,. \tag{4.10}$$

If the director is the ground state for a cholesteric, given by equation (2.11), then the dielectric tensor will be given by

$$\underline{\underline{\epsilon}} = \epsilon_\perp \underline{\underline{\delta}} + \epsilon_a \begin{pmatrix} \cos^2\phi & \cos\phi\sin\phi & 0 \\ \cos\phi\sin\phi & \sin^2\phi & 0 \\ 0 & 0 & 0 \end{pmatrix} . \tag{4.11}$$

It is easy to show by trigonometric identities that this is equivalent to

$$\underline{\underline{\epsilon}} = \bar{\epsilon}\underline{\underline{\delta}} + \frac{\epsilon_a}{2} \begin{pmatrix} \cos 2\phi & \sin 2\phi & 0 \\ \sin 2\phi & -\cos 2\phi & 0 \\ 0 & 0 & -1 \end{pmatrix} , \tag{4.12}$$

where $\bar{\epsilon} = (\epsilon_\parallel + \epsilon_\perp)/2$. Equation (4.10) can easily be inverted, and using equation (2.11), can be shown to yield

$$\underline{\underline{\epsilon}}^{-1} = \frac{1}{\bar{\epsilon}^2 - (\epsilon_a/2)^2} \left[ \bar{\epsilon}\underline{\underline{\delta}} - \frac{\epsilon_a}{2} \begin{pmatrix} \cos 2\phi & \sin 2\phi & 0 \\ \sin 2\phi & -\cos 2\phi & 0 \\ 0 & 0 & -1 \end{pmatrix} \right] . \tag{4.13}$$

Much like equation (4.11), equation (4.13) can be rewritten in the form

$$\underline{\underline{\epsilon}}^{-1} = b \left[ \underline{\underline{\delta}} - \alpha \begin{pmatrix} \cos 2\phi & \sin 2\phi & 0 \\ \sin 2\phi & -\cos 2\phi & 0 \\ 0 & 0 & -1 \end{pmatrix} \right] , \tag{4.14}$$

where $\alpha = \frac{\epsilon_\parallel - \epsilon_\perp}{\epsilon_\parallel + \epsilon_\perp}$ and $b = \frac{1}{2}\left(\frac{1}{\epsilon_\parallel} + \frac{1}{\epsilon_\perp}\right)$.

Thus, in this system, the displacement field is given by

$$\mathbf{D} = \begin{pmatrix} \bar{\epsilon} + (\epsilon_a/2)\cos(2\phi) & (\epsilon_a/2)\sin(2\phi) \\ (\epsilon_a/2)\sin(2\phi) & \bar{\epsilon} - (\epsilon_a/2)\cos(2\phi) \end{pmatrix} \mathbf{E} . \tag{4.15}$$

De Vries was first to propose the method of solving equation (4.9) for light normally incident on a CLC at any frequency by transforming $\mathbf{E}(z)$ into a coordinate frame which rotates along with the dielectric tensor, so that the matrix connecting $\mathbf{D}$ with $\mathbf{E}$ is diagonal

[19]. Given that $\phi = qz$ *, I can define the rotating coordinate system $(\xi, \eta)$ such that

$$\begin{pmatrix} E_x \\ E_y \end{pmatrix} = \begin{pmatrix} \cos(qz) & -\sin(qz) \\ \sin(qz) & \cos(qz) \end{pmatrix} \begin{pmatrix} E_\xi \\ E_\eta \end{pmatrix} \tag{4.16}$$

which yields the result that

$$D_\xi = (\bar{\epsilon} + \epsilon_a/2)E_\xi = \epsilon_\parallel E_\xi \tag{4.17}$$

$$D_\eta = (\bar{\epsilon} - \epsilon_a/2)E_\eta = \epsilon_\perp E_\eta \, . \tag{4.18}$$

If I substitute the transformation (4.16) into equation (4.9), I can combine terms to obtain the eigen-like equation,

$$\left(\frac{\omega}{c}\right)^2 \begin{pmatrix} \epsilon_\parallel E_\xi \\ \epsilon_\perp E_\eta \end{pmatrix} = -\begin{pmatrix} \partial_z^2 - q^2 & -2q\partial_z \\ 2q\partial_z & \partial_z^2 - q^2 \end{pmatrix} \begin{pmatrix} E_\xi \\ E_\eta \end{pmatrix} \, . \tag{4.19}$$

Note that in this rotating coordinate system, even a state with $\partial_z E_\xi = 0$ and $\partial_z E_\eta = 0$ has a non-zero energy $\omega = cq$, arising from the variations in $\mathbf{B}$ and $\mathbf{E}$ associated with the frame rotation. Since equation (4.19) has constant coefficients, I can guess that both components can be described by a single plane-wave of the form $\mathbf{E} \sim \exp[i\,(kz - \omega t)]$. The most generic solution has an elliptical polarisation, parameterised by

$$E_\xi = A \exp[i\,(kz - \omega t)] \tag{4.20}$$

$$E_\eta = iB \exp[i\,(kz - \omega t)] \, . \tag{4.21}$$

One can substitute these expressions into equation (4.19) to obtain the matrix equation

$$\begin{pmatrix} \epsilon_\parallel \left(\frac{\omega}{c}\right)^2 - q^2 - k^2 & -2iqk \\ -2iqk & \epsilon_\perp \left(\frac{\omega}{c}\right)^2 - q^2 - k^2 \end{pmatrix} \begin{pmatrix} A \\ iB \end{pmatrix} = \begin{pmatrix} 0 \\ 0 \end{pmatrix} \, , \tag{4.22}$$

The eigenvalues $\lambda$ of the 2 by 2 square matrix in equation (4.22) yield an implicit expression for $k$, and the eigenvectors yield the ratio of the polarisations, $A/B$.

$$\zeta = -k^2 - q^2 + \bar{\epsilon}\left(\frac{\omega}{c}\right)^2 \pm \frac{1}{2}\sqrt{\epsilon_a^2\left(\frac{\omega}{c}\right)^4 + 16k^2q^2} \tag{4.23}$$

$$\frac{A}{B} = \frac{1}{4kq}\left[\epsilon_a\left(\frac{\omega}{c}\right)^2 \mp \sqrt{\epsilon_a^2\left(\frac{\omega}{c}\right)^4 + 16k^2q^2}\right] \, . \tag{4.24}$$

*In the case of an unperturbed cholesteric, $\phi = q_0 z$, but I use $q$ which is correct even under a contraction $\lambda_{zz}$ along the $z$ direction.

*Reduction to Dimensionless Units*

Equations (4.19-4.24) can be rewritten in a dimensionless form that increases the universality of the results. A clever choice of reductions will also simplify the expressions to a more tractable form. The natural wavenumber to choose for the reduction is $q$, and the natural velocity is $c$. In the first approximation, just based on dimensional analysis, one might pick a reduced wavevector $\tilde{k} = k/q$ and a reduced frequency $\tilde{\omega} = \omega/cq$. However, recalling that the vectors $\mathbf{n}$ and $-\mathbf{n}$ are indistinguishable, the actual period of the liquid crystal is halved, and the actual "natural" wavenumber is doubled to $2q$. That means that the proper choice for reduction of the wavevector is $\tilde{k} = k/2q$. In preparation for the next chapter, I also note here that this analysis means that the reciprocal lattice vectors in a CLC will be given by $\mathbf{G} = 2nq\hat{z}$, where $n$ is an integer multiple of the "natural" unit wavenumber. However, there is another complication. Rather than the absolute values of refractive indices, the most interesting parameter is generally the refractive index contrast $\alpha$, which is defined above. Two systems with different $\epsilon_{\parallel}$ and $\epsilon_{\perp}$, but the same values for $\alpha$, will have virtually the same optical properties, except for a pre-factor. The best way to eliminate this pre-factor is to incorporate it into the frequency. It is clear from inspection of equations (4.8) and (4.14), that the constant $b$ in equation (4.14) will factor out on the left-hand side of equation (4.8) and can be incorporated into the reduced frequency, such that $\tilde{\omega} = \omega/2cq\sqrt{b}$.

In these new reduced units, the eigensystem in equation (4.22) may be rewritten as

$$\begin{pmatrix} \frac{4}{1-\alpha}\tilde{\omega}^2 - 4\tilde{k}^2 - 1 & -4i\tilde{k} \\ 4i\tilde{k} & \frac{4}{1+\alpha}\tilde{\omega}^2 - 4\tilde{k}^2 - 1 \end{pmatrix} \begin{pmatrix} A \\ iB \end{pmatrix} = \begin{pmatrix} 0 \\ 0 \end{pmatrix}, \tag{4.25}$$

which yields the solutions

$$\lambda = -1 - 4\tilde{k}^2 + \frac{4\alpha\tilde{\omega}^2 \pm \sqrt{(1-\alpha^2)^2\,\tilde{k}^2 + \alpha^2\tilde{\omega}^4}}{1-\alpha^2} \tag{4.26}$$

$$\frac{A}{B} = \frac{\alpha\tilde{\omega}^2 \pm \sqrt{\tilde{k}^2\,(1-\alpha^2)^2 + \alpha^2\tilde{\omega}^4}}{\tilde{k}(1-\alpha^2)} \tag{4.27}$$

Setting $\lambda = 0$ yields the dispersion relation

$$\tilde{\omega} = \pm\frac{1}{2}\sqrt{1 + 4\tilde{k}^2 \pm \sqrt{16\alpha^2\tilde{k}^4 + 8(2-\alpha^2)\tilde{k}^2 + \alpha^2}}\,. \tag{4.28}$$

The upper branches may be used directly to plot the functional dependence of $\tilde{\omega}$ on $\tilde{k}$, as shown in figure 4.1.

It is evident that there is one gap in the dispersion relation when $\tilde{k} = 0$, which

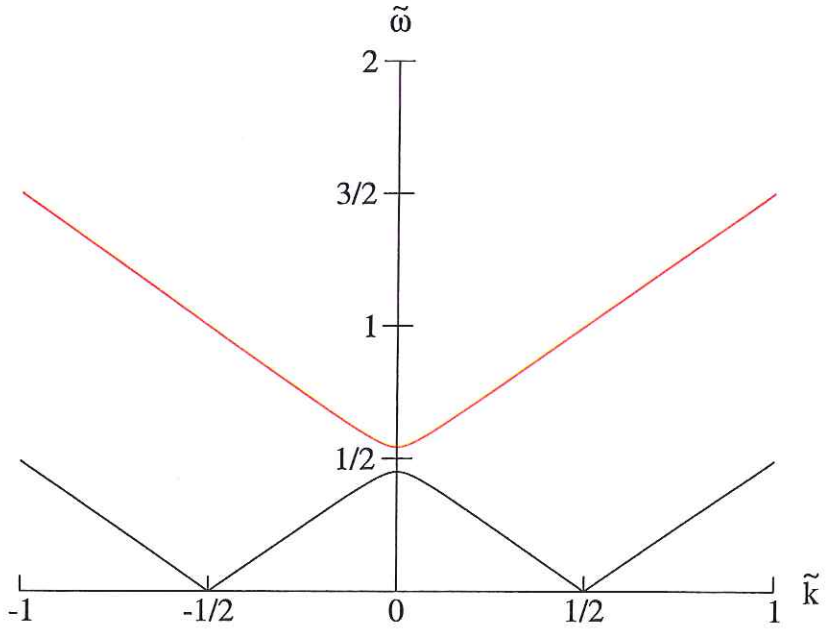


Figure 4.1: Dispersion relation for an ideal helix, calculated from equation (4.28) with $\alpha = 0.18$. There is a single gap for one polarisation, at $\tilde{k} = 0$, and no gap for the other polarisation.

is an eigenstate corresponding to the coherent superposition of two plane waves with wavevectors of $\pm 1/2$ in reduced units [20]. Equation (4.28) also implies that the lower branch will have a reduced frequency $\tilde{\omega}_l = \frac{1}{2}\sqrt{1-\alpha}$ and $B/A = 0$, while the upper branch will have a reduced frequency $\tilde{\omega}_u = \frac{1}{2}\sqrt{1+\alpha}$ and $A/B = 0$. This data means that both eigenmodes at the band gap are linearly polarised. The difference between the two is that the lower branch points wholly along the rotating $\xi$ axis, with an effective dielectric constant $1/(1-\alpha)$ in reduced units, while the upper branch points along the rotating $\eta$ axis, with an effective dielectric constant $1/(1+\alpha)$. This range of forbidden frequencies is referred to as the band gap. † Bloch's theorem ensures that states intermediate in frequency and polarisation between the upper and lower branches are forbidden, i.e., will decay exponentially in the bulk. This principle is illustrated in figure 4.2, a more conventional dispersion relation which is plotted as a single-valued function $\omega(\mathbf{k})$, which may be obtained by eliminating the parts of figure 4.1 with negative group velocity (i.e., $d\omega/dk < 0$).

Of course, it is necessary to understand how these solutions inside the cholesteric translate into a solution outside the cholesteric. The solution, obviously, is that the two eigenstates inside the cholesteric correspond to left and right-handed circularly polarised

†There is only one gap. In the degenerate perturbation analysis for gap scaling in distorted cholesterics of section 5.3.2, I discuss why simple cholesterics only have one gap.

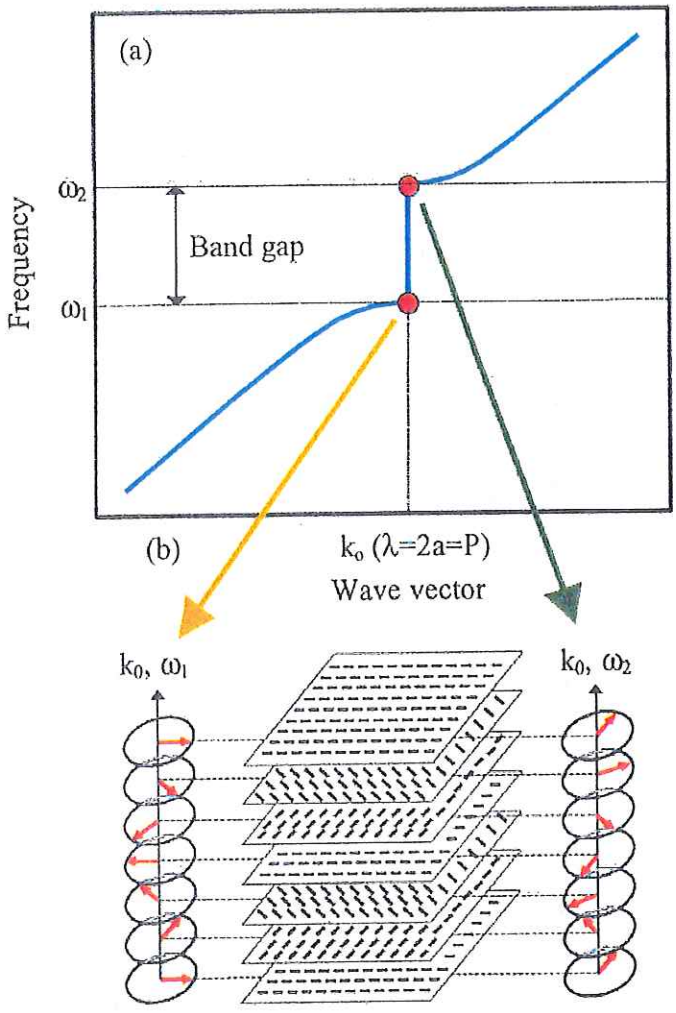


Figure 4.2: Illustration of the polarisations of the upper and lower branches of the dispersion relation at the band gap (adapted from reference [37]).

light outside the cholesteric. The eigenstate which is split by a band gap is clearly the one that rotates in the same direction of the helix. That is why cholesterics are observed to reflect light with one sense of circular polarisation, and to reflect it with the same sense, while light polarised with the opposite circular polarisation is transmitted unaffected.

I can show this explicitly by the analysis of boundary conditions, assuming the cholesteric is a semi-infinite medium, which borders on a homogeneous dielectric medium at $z = 0$ of dielectric constant $\bar{\epsilon}$. By Gauss' law for dielectrics, I know that the flux through a Gaussian surface enclosing the boundary is proportional to the free charge enclosed. Since it is zero by assumption, the flux contribution above and below the boundary must be equal. That can only be true if $(\mathbf{D}_{\|})_{\text{above}} = (\mathbf{D}_{\|})_{\text{below}}$, or in my case, $\lim_{\delta \to 0} \; [\mathbf{D}(-\delta) - \mathbf{D}(\delta)] \cdot \hat{z} = 0$. Of course, since I know that $\mathbf{D} \cdot \hat{z} = 0$ for normally incident light, the first boundary

condition just says that the light remains normally incident once it enters the cholesteric medium (cf. Snell's law).

Secondly, by Ampere's law, I know that a closed line integral of the magnetic field must be proportional to the enclosed free current. Since I have no free current at the boundary by assumption, I must have an equal contribution from the magnetic fields above and below the boundary, much like before. This time, that implies that $(\mathbf{H}_\perp)_{\text{above}} = (\mathbf{H}_\perp)_{\text{below}}$. Since my cholesteric and homogeneous media have $\mu_r = 1$, I can use equation (4.3) to say that such a condition is equivalent to the statement that the curl of $\mathbf{E}$ must be unchanged across the boundary. Numerical analysis shows that light which is locally linearly polarised and follows the helix will correspond exactly to a circularly polarised state in the homogeneous medium. Of course, in general the polarisation of light propagating through a cholesteric medium will be elliptical, with semi-minor and semi-major axes corresponding to the principal axes of the dielectric tensor. The corresponding eigenstates outside the medium will be again two opposite circular polarisations to within a factor of order $\alpha$ for all frequencies, as shown in de Vries' original work [19]. This can also be shown numerically.

Alternatively, one can solve equation (4.19) using de Vries' original notation for the solutions, which is

$$E_\xi = A \exp\left[2\pi i \left(\frac{t}{T} - \frac{mz}{\lambda}\right)\right] \tag{4.29}$$

$$E_\eta = iB \exp\left[2\pi i \left(\frac{t}{T} - \frac{mz}{\lambda}\right)\right], \tag{4.30}$$

where $T$ is the period of the wave, $\lambda$ is the wavelength *in vacuo*, and $m$ is the effective refractive index. I can then reduce the latter two quantities according to the transformations $\lambda \to \lambda' = \lambda/p_0\sqrt{\bar{\epsilon}}$ and $m \to m' = m/\sqrt{\bar{\epsilon}}$. I obtain the solution

$$m'^2 = 1 + \lambda'^2 \pm \sqrt{(1+\lambda'^2)^2 - (1-\alpha-\lambda'^2)(1+\alpha-\lambda'^2)} \tag{4.31}$$

$$\frac{B}{A} = \frac{1-\alpha-m'^2-\lambda^2}{2m'\lambda'}. \tag{4.32}$$

It is clear from equation (4.31) that the smaller value of $m'^2$ will be negative for values of $\lambda' \approx 1$, such that $1-\alpha < \lambda'^2 < 1+\alpha$. This yields an imaginary value for $m'$, corresponding to an exponentially decaying (forbidden) wave. Conversely, the larger solution for $m'$ is always real, as can be seen by inspection, and thus will always propagate in the bulk.

The usual interpretation of these results is that there is a range of wavelengths, such that $1-\alpha < \lambda'^2 < 1+\alpha$, within which only one polarisation of light is reflected. The de Vries result is equivalent to my findings, discussed previously.

## 4.2 Distorted Helix

Looking back at the derivation of equation (4.22), it is clear that it works only for the case where $\phi = q_0 z$; however, that only holds true for the case of an ideal helix. If any external fields are imposed on the medium, e.g., an external electric or magnetic field, as discussed in section 2.5, or mechanical strain, as explained in section 3.3, then the simple, linear relationship between $\phi$ and $z$ will fail.

The obvious extension of de Vries' technique for solving equation (4.9) for a CLC consists in transforming into a set of rotating coordinates defined in a way that generalises from the case where $\phi = q_0 z$ to an arbitrary function $\phi = \phi(z)$. This is written as:

$$\begin{pmatrix} E_x \\ E_y \end{pmatrix} = \begin{pmatrix} \cos\phi & -\sin\phi \\ \sin\phi & \cos\phi \end{pmatrix} \begin{pmatrix} E_\xi \\ E_\eta \end{pmatrix} . \tag{4.33}$$

I can then insert this expression into equations (4.9) and (4.15) to obtain the relation

$$\left(\frac{\omega}{c}\right)^2 \begin{pmatrix} \epsilon_\parallel E_\xi \\ \epsilon_\perp E_\eta \end{pmatrix} = \begin{pmatrix} \phi'^2 - \partial_z^2 & 2\phi'\partial_z + \phi'' \\ -2\phi'\partial_z - \phi'' & \phi'^2 - \partial_z^2 \end{pmatrix} \begin{pmatrix} E_\xi \\ E_\eta \end{pmatrix} . \tag{4.34}$$

Substitution of $\phi = q_0 z$ into equation (4.34) recovers equation (4.19), as expected. However, there are evidently two problems with equation (4.34): (1) the rotating coordinate system rotates at a non-uniform rate for a generalised $\phi$, and (2) the expressions for $\phi'$ and $\phi''$ are in general non-trivial functions of $z$, as illustrated in figures 2.3 and 3.2. That means that I cannot find an analytical solution in general for an arbitrary $\phi(z)$. Nonetheless, equation (4.34) will still be amenable to numerical solution, and may be useful in the analysis of systems with an aperiodic $\phi(z)$. Examples of experimental relevance include spatially varying cholesteric solids with large-scale inhomogeneities resulting from a temperature or concentration gradient, and cholesteric liquids which are used as filters. Although this is an interesting and largely unexplored possibility, I will not pursue this topic further within this thesis.

# Chapter 5

# CLC Optics: Band Structure Approach

In the previous section, I established the need to develop another technique to calculate the optical properties of a cholesteric, due to the complexity of the equations governing the propagation of light. The solution presented in this thesis is to apply the tools of electronic structure theory to calculate photonic band structures.

## 5.1 General Photonic Band Theory

According to Bloch's theorem, any wave propagating through a periodic structure is given by the product of a periodic function and a plane wave, indexed by a wavevector $\mathbf{k}$. From the set of operations under which the system is invariant, one can construct a set of reciprocal lattice vectors, $\{\mathbf{G}\}$. The index wavevector $\mathbf{k}$ is unique only modulo a reciprocal lattice vector, which thus limits the number of values of $\mathbf{k}$ which must be explored in order to fully characterise the dispersion relation of the medium. One may use the perpendicular bisectors of the reciprocal lattice vectors to construct Wigner-Seitz cells, known as Brillouin zones. Since $\mathbf{k}$ is non-unique, if one calculates the dispersion relation within one Brillouin zone, typically the one centered on the origin known as the first Brillouin zone, all others will be determined. Furthermore, the point-group symmetries of the system will often allow one to reduce the number of $\mathbf{k}$ values which must be explored. The minimum set consistent with a complete characterisation of the system is known as the irreducible Brillouin zone. Because of the periodicity of the structure, if a frequency is found nowhere on the dispersion curves in the irreducible Brillouin zone, it is said to be forbidden. Thus, calculating the bands resulting from traversing the irreducible Brillouin zone is considered equivalent to solving the electronic or photonic structure of the system.

In electronic structure theory, materials which have band gaps around the Fermi level

act as insulators, since the electrons need a relatively large amount of energy to be excited into delocalised states, known as conduction bands. In photonics, one seeks to understand what happens to monochromatic light incident on a periodic dielectric structure. The standard interpretation of photonic band structures is that a band gap corresponds to a range of frequencies which are wholly reflected by the photonic medium (ignoring absorption losses).

I choose to adapt the technique for calculating optical band structures, originally devised by Ho, Chan and Soukoulis [11] and refined by Meade and colleagues [24], to calculate the properties of light propagating through any arbitrary periodic dielectric medium. Although both groups implicitly assume that the dielectric constant is a piecewise continuous, scalar quantity, I generalise to the case of a tensor dielectric constant where the polarisation, and its rotation, lead to new, subtle effects.

I start with Maxwell's equations in wave form, rewritten here for clarity:

$$\nabla \times \left[\underline{\underline{\epsilon}}^{-1}(\mathbf{r})(\nabla \times \mathbf{H})\right] = -\frac{1}{c^2}\frac{\partial^2 \mathbf{H}}{\partial t^2} \,. \tag{5.1}$$

If I assume that $\mathbf{H}(\mathbf{r},t) = \mathbf{H}(\mathbf{r})e^{i\omega t}$, I can rewrite equation (5.1) as:

$$\nabla \times \left[\underline{\underline{\epsilon}}^{-1}(\mathbf{r})\,(\nabla \times \mathbf{H})\right] = \left(\frac{\omega}{c}\right)^2 \mathbf{H} \,. \tag{5.2}$$

Since the dielectric tensor is periodic by assumption, I have $\underline{\underline{\epsilon}}(\mathbf{r}) = \underline{\underline{\epsilon}}(\mathbf{r}+\mathbf{T})$, where $\mathbf{T} = np_0\hat{z}$ with $n$ integer in a cholesteric, and $\mathbf{T} = \sum_{i=1}^{3} n_i \mathbf{a}_i$ with $n_i$ integer in general. I can then define a translation operator $\hat{\mathcal{T}}_{\mathbf{T}}$, which has the property that

$$\hat{\mathcal{T}}_{\mathbf{T}} f(\mathbf{r}) = f(\mathbf{r}+\mathbf{T}) \tag{5.3}$$

If I then define the "Maxwell operator" $\hat{\mathcal{M}}$ such that

$$\hat{\mathcal{M}}\mathbf{H}(\mathbf{r}) = \nabla \times \left[\underline{\underline{\epsilon}}^{-1}(\mathbf{r})(\nabla \times \mathbf{H}(\mathbf{r}))\right] \,, \tag{5.4}$$

then equation (5.2) can be rewritten simply as

$$\hat{\mathcal{M}}\mathbf{H}(\mathbf{r}) = \left(\frac{\omega}{c}\right)^2 \mathbf{H}(\mathbf{r}) \,. \tag{5.5}$$

The translation operator applied to the left-hand side of equation (5.5) yields:

$$\hat{\mathcal{T}}_{\mathbf{T}} \left(\hat{\mathcal{M}}(\mathbf{r})\mathbf{H}(\mathbf{r})\right) = \left(\hat{\mathcal{T}}_{\mathbf{T}}\hat{\mathcal{M}}\right)\left(\hat{\mathcal{T}}_{\mathbf{T}}\mathbf{H}(\mathbf{r})\right) \,. \tag{5.6}$$

Since $\hat{\mathcal{T}}_{\mathbf{T}}\hat{\mathcal{M}} = \hat{\mathcal{M}}$, owing to the periodicity of $\underline{\underline{\epsilon}}(\mathbf{r})$, I can remove the operands from

equation (5.6) to show that $\hat{\mathcal{T}}_{\mathbf{T}}\hat{\mathcal{M}} - \hat{\mathcal{M}}\hat{\mathcal{T}}_{\mathbf{T}} = 0$, i.e., the operators $\hat{\mathcal{T}}_{\mathbf{T}}$ and $\hat{\mathcal{M}}$ commute. By the fundamental postulates of linear algebra [illegible], I know that any pair of operators which commute can be chosen to have the same eigenstates, so that

$$\hat{\mathcal{M}}\mathbf{H}(\mathbf{r}) = \left(\frac{\omega}{c}\right)^2 \mathbf{H}(\mathbf{r}) \tag{5.7}$$

$$\hat{\mathcal{T}}_{\mathbf{T}}\mathbf{H}(\mathbf{r}) = c(\mathbf{T})\mathbf{H}(\mathbf{r}) \,. \tag{5.8}$$

I can now define a wavevector $\mathbf{k}$ such that $c(\mathbf{T}) = e^{i\mathbf{k}\cdot\mathbf{T}}$. Clearly, then, I can rewrite equation (5.8) as

$$\mathbf{H}(\mathbf{r}+\mathbf{T}) = e^{i\mathbf{k}\cdot\mathbf{T}}\mathbf{H}(\mathbf{r}) \,. \tag{5.9}$$

Since this property should be true for all translations, I can expand equation (5.9) into

$$\mathbf{H}(\mathbf{r}) = e^{i\mathbf{k}\cdot\mathbf{r}}\mathbf{h}(\mathbf{r}) \tag{5.10}$$

$$\mathbf{h}(\mathbf{r}+\mathbf{T}) = \mathbf{h}(\mathbf{r}) \,. \tag{5.11}$$

Equations (5.10-5.11) show explicitly that the solutions to equation (5.2) are guaranteed to be the product of a plane wave times a periodic function. By the Fourier theorem, I can rewrite the periodic function $\mathbf{h}(\mathbf{r})$ as a sum of Fourier components

$$\mathbf{h}(\mathbf{r}) = \sum_{\mathbf{G}} \mathbf{h}_{\mathbf{G}} e^{i\mathbf{G}\cdot\mathbf{r}} \,, \tag{5.12}$$

where $\{\mathbf{G}\}$ is the set of all reciprocal lattice vectors, defined such that $e^{i\mathbf{G}\cdot\mathbf{T}} = 1$. Inserting into equation (5.10), I find

$$\mathbf{H}(\mathbf{r}) = e^{i\mathbf{k}\cdot\mathbf{r}} \sum_{\mathbf{G}} \mathbf{h}_{\mathbf{G}} e^{i\mathbf{G}\cdot\mathbf{r}} \,, \tag{5.13}$$

or, rearranging,

$$\mathbf{H}(\mathbf{r}) = \sum_{\mathbf{G}} \mathbf{h}_{\mathbf{G}} e^{i(\mathbf{k}+\mathbf{G})\cdot\mathbf{r}} \,. \tag{5.14}$$

Since equation (4.2) guarantees that $\mathbf{H}$ is transverse, I can pick two basis vectors $\hat{e}_{(\mathbf{G}\gamma)}$ of magnitude one for each $\mathbf{G}$ such that

$$\forall_{(\mathbf{G}\gamma)} \left[\hat{e}_{(\mathbf{G}\gamma)} \cdot (\mathbf{k}+\mathbf{G})\right] = 0 \,, \tag{5.15}$$

and

$$\forall_{(\mathbf{G}\gamma\gamma')}\left[\hat{e}_{(\mathbf{G}\gamma)}\cdot\hat{e}_{(\mathbf{G}\gamma')}\right]=\delta_{\gamma,\gamma'}\ . \tag{5.16}$$

Thus $\mathbf{k}+\mathbf{G}$ and the $\hat{e}_{(\mathbf{G}\gamma)}$ form an orthogonal triad of vectors in space for each $\mathbf{G}$, and the $\hat{e}_{(\mathbf{G}\gamma)}$ may be different for each $\mathbf{G}$ in general. Each plane-wave component of $\mathbf{H}$ is thus guaranteed to point in the plane created by the $\hat{e}_{(\mathbf{G}\gamma)}$. This result allows us to rewrite equation (5.14) as

$$\mathbf{H}(\mathbf{r})=\sum_{\mathbf{G}}\sum_{\gamma=1}^{2}h_{(\mathbf{G}\gamma)}\hat{e}_{(\mathbf{G}\gamma)}e^{i(\mathbf{k}+\mathbf{G})\cdot\mathbf{r}}\ . \tag{5.17}$$

Equation (5.17) is my Fourier representation of the $\mathbf{H}$ field. I would now like to insert this expression into equation (5.2) so as to transform my eigen-like operator problem into an eigenvalue equation, with an effective matrix derived from the Maxwell operator $\hat{\mathcal{M}}$. The reason that I can do that now is that the curl operator is diagonal in Fourier space. However, I cannot get very far without noticing the inverse dielectric tensor is not diagonal under the curl operator in general. Fortunately, I can easily fix this problem. Applying the Fourier theorem, I expand $\underline{\underline{\epsilon}}^{-1}$ in a plane-wave basis set such that

$$\underline{\underline{\epsilon}}^{-1}(\mathbf{r})=\sum_{\mathbf{G}'}\underline{\underline{\epsilon}}^{-1}_{\mathbf{G}}\,e^{i\mathbf{G}'\cdot\mathbf{r}}\ . \tag{5.18}$$

I can now substitute equations (5.17) and (5.18) into equation (5.2) to obtain

$$\begin{aligned}&\left(\frac{\omega}{c}\right)^2\sum_{\mathbf{G}}\sum_{\gamma=1}^{2}\hat{e}_{(\mathbf{G}\gamma)}h_{(\mathbf{G}\gamma)}e^{i(\mathbf{k}+\mathbf{G})\cdot\mathbf{r}}= \\ &-\sum_{\mathbf{G},\mathbf{G}'}\sum_{\gamma=1}^{2}h_{(\mathbf{G}\gamma)}(\mathbf{k}+\mathbf{G}+\mathbf{G}')\times\left\{\underline{\underline{\epsilon}}^{-1}_{\mathbf{G}'}\cdot\left[(\mathbf{k}+\mathbf{G})\times\hat{e}_{(\mathbf{G}\gamma)}\right]\right\}e^{i(\mathbf{k}+\mathbf{G}+\mathbf{G}')\cdot\mathbf{r}}\ ,\end{aligned} \tag{5.19}$$

upon which I can effect the transformation $\mathbf{G}'\rightarrow\mathbf{G}'-\mathbf{G}$. That procedure gives us

$$\begin{aligned}&\left(\frac{\omega}{c}\right)^2\sum_{\mathbf{G}}\sum_{\gamma=1}^{2}\hat{e}_{(\mathbf{G}\gamma)}h_{(\mathbf{G}\gamma)}e^{i(\mathbf{k}+\mathbf{G})\cdot\mathbf{r}}= \\ &-\sum_{\mathbf{G},\mathbf{G}'}\sum_{\gamma=1}^{2}h_{(\mathbf{G}\gamma)}(\mathbf{k}+\mathbf{G}')\times\left\{\underline{\underline{\epsilon}}^{-1}_{\mathbf{G}'-\mathbf{G}}\cdot\left[(\mathbf{k}+\mathbf{G})\times\hat{e}_{(\mathbf{G}\gamma)}\right]\right\}e^{i(\mathbf{k}+\mathbf{G}')\cdot\mathbf{r}}\ .\end{aligned} \tag{5.20}$$

Multiplying by $e^{-i(\mathbf{k}+\mathbf{G}_0)\cdot\mathbf{r}}$, and integrating over the unit cell, I obtain

$$\left(\frac{\omega}{c}\right)^2 \sum_{\gamma} h_{(\mathbf{G}'\gamma)}\hat{e}_{(\mathbf{G}'\gamma)} = -\sum_{\mathbf{G}}\sum_{\gamma} h_{(\mathbf{G}\gamma)}(\mathbf{k}+\mathbf{G}')\times\left\{\underline{\underline{\epsilon}}^{-1}_{\mathbf{G}'-\mathbf{G}}\cdot\left[(\mathbf{k}+\mathbf{G})\times\hat{e}_{(\mathbf{G}\gamma)}\right]\right\} \ . \quad (5.21)$$

The structure of equation (5.21) ensures that there is a solution. One reason is that since the last operation on the right- hand side of equation (5.21) is a cross-product with $\mathbf{k}+\mathbf{G}'$, it will automatically have components along $\hat{e}_{(\mathbf{G}'\gamma)}$, which are contained in the left-hand side.

Clearly, if I multiply equation (5.21) by $\hat{e}_{(\mathbf{G}\gamma)'}$, and assume without loss of generality that

$$\begin{aligned}(\mathbf{k}+\mathbf{G})\times\hat{e}_{(\mathbf{G}1)} &= \hat{e}_{(\mathbf{G}2)} \\ (\mathbf{k}+\mathbf{G})\times\hat{e}_{(\mathbf{G}2)} &= -\hat{e}_{(\mathbf{G}1)} \ ,\end{aligned} \quad (5.22)$$

I obtain

$$\begin{aligned}\left(\frac{\omega}{c}\right)^2 h_{(\mathbf{G}\gamma)'} = -\,|\mathbf{k}+\mathbf{G}|\sum_{\mathbf{G}} & h_{(\mathbf{G}1)}\hat{e}_{(\mathbf{G}\gamma)'}\cdot\left[(\mathbf{k}+\mathbf{G}')\times\left(\underline{\underline{\epsilon}}^{-1}_{\mathbf{G}'-\mathbf{G}}\cdot\hat{e}_{(\mathbf{G}2)}\right)\right] \\ & -h_{(\mathbf{G}2)}\hat{e}_{(\mathbf{G}\gamma)'}\cdot\left[(\mathbf{k}+\mathbf{G}')\times\left(\underline{\underline{\epsilon}}^{-1}_{\mathbf{G}'-\mathbf{G}}\cdot\hat{e}_{(\mathbf{G}1)}\right)\right] \ .\end{aligned} \quad (5.23)$$

Equation (5.23) demonstrates that there is a matrix that links the $h_{(\mathbf{G}\gamma)}$ across $\mathbf{G}$ and $\gamma$ space. If I define a doublet $\mathbf{h}$ such that $\mathbf{h}_{\mathbf{G}} = \begin{pmatrix} h_{(\mathbf{G}1)} \\ h_{(\mathbf{G}2)} \end{pmatrix}$, then I can combine equation (5.23) to write the matrix equation

$$\left(\frac{\omega}{c}\right)^2 \mathbf{h}_{\mathbf{G}'} = \sum_{\mathbf{G}} \underline{\underline{A}}_{\mathbf{G}',\mathbf{G}}\mathbf{h}_{\mathbf{G}} \ , \quad (5.24)$$

where $\underline{\underline{A}}_{\mathbf{G}',\mathbf{G}}$ is given by

$$\begin{aligned}\underline{\underline{A}}_{\mathbf{G}',\mathbf{G}} = & -|\mathbf{k}+\mathbf{G}| \\ & \begin{pmatrix} \hat{e}_{(\mathbf{G}'1)}\cdot\left[(\mathbf{k}+\mathbf{G}')\times\left(\underline{\underline{\epsilon}}^{-1}_{\mathbf{G}'-\mathbf{G}}\cdot\hat{e}_{(\mathbf{G}2)}\right)\right] & -\hat{e}_{(\mathbf{G}'1)}\cdot\left[(\mathbf{k}+\mathbf{G}')\times\left(\underline{\underline{\epsilon}}^{-1}_{\mathbf{G}'-\mathbf{G}}\cdot\hat{e}_{(\mathbf{G}1)}\right)\right] \\ \hat{e}_{(\mathbf{G}'2)}\cdot\left[(\mathbf{k}+\mathbf{G}')\times\left(\underline{\underline{\epsilon}}^{-1}_{\mathbf{G}'-\mathbf{G}}\cdot\hat{e}_{(\mathbf{G}2)}\right)\right] & -\hat{e}_{(\mathbf{G}'2)}\cdot\left[(\mathbf{k}+\mathbf{G}')\times\left(\underline{\underline{\epsilon}}^{-1}_{\mathbf{G}'-\mathbf{G}}\cdot\hat{e}_{(\mathbf{G}1)}\right)\right] \end{pmatrix} .\end{aligned} \quad (5.25)$$

## 5.2 Special Cases for Band Structure Calculations

### 5.2.1 1D periodic structure, normal incidence

In the case where I have a 1-D periodic structure, I can simplify equation (5.25). In particular, if the periodicity is along the $z$ axis, and I only consider normal incidence, then it is clear that my two unit vectors $\hat{e}_{(\mathbf{G}\gamma)}$ will lie in the $xy$ plane, which allows us to make the choice without loss of generality that $\forall_{\mathbf{G}}\ \hat{e}_{(\mathbf{G}1)} = \hat{x}$ and $\forall_{\mathbf{G}}\ \hat{e}_{(\mathbf{G}2)} = \hat{y}$. In this case, it is obvious from equation (5.25) that the $z$ components of $\underline{\underline{\epsilon}}^{-1}$ will be suppressed, which allows me to write that

$$\underline{\underline{\epsilon}}^{-1}_{\mathbf{G}'-\mathbf{G}} = \begin{pmatrix} (\underline{\underline{\epsilon}}^{-1}_{\mathbf{G}'-\mathbf{G}})_{xx} & (\underline{\underline{\epsilon}}^{-1}_{\mathbf{G}'-\mathbf{G}})_{xy} \\ (\underline{\underline{\epsilon}}^{-1}_{\mathbf{G}'-\mathbf{G}})_{yx} & (\underline{\underline{\epsilon}}^{-1}_{\mathbf{G}'-\mathbf{G}})_{yy} \end{pmatrix} . \tag{5.26}$$

I can apply equation (5.26) to equation (5.25) to obtain the result that

$$\underline{\underline{A}}_{\mathbf{G}',\,\mathbf{G}} = |\mathbf{k}+\mathbf{G}|\ |\mathbf{k}+\mathbf{G}'| \begin{pmatrix} (\underline{\underline{\epsilon}}^{-1}_{\mathbf{G}'-\mathbf{G}})_{yy} & -(\underline{\underline{\epsilon}}^{-1}_{\mathbf{G}'-\mathbf{G}})_{yx} \\ -(\underline{\underline{\epsilon}}^{-1}_{\mathbf{G}'-\mathbf{G}})_{xy} & (\underline{\underline{\epsilon}}^{-1}_{\mathbf{G}'-\mathbf{G}})_{xx} \end{pmatrix} . \tag{5.27}$$

I then recall the reduced expression for $\underline{\underline{\epsilon}}^{-1}$, equation (4.14).

$$\underline{\underline{\epsilon}}^{-1} = b \left[ \underline{\underline{\delta}} - \alpha \begin{pmatrix} \cos 2\phi & \sin 2\phi & 0 \\ \sin 2\phi & -\cos 2\phi & 0 \\ 0 & 0 & -1 \end{pmatrix} \right] , \tag{5.28}$$

The Fourier components for $\underline{\underline{\epsilon}}$ will be given by

$$\underline{\underline{\epsilon}}^{-1}_{\mathbf{G}'-\mathbf{G}} = b \begin{pmatrix} \delta_{\mathbf{G}\mathbf{G}'} - \alpha c_{\mathbf{G}'-\mathbf{G}} & -\alpha s_{\mathbf{G}'-\mathbf{G}} & 0 \\ -\alpha s_{\mathbf{G}'-\mathbf{G}} & \delta_{\mathbf{G}\mathbf{G}'} + \alpha c_{\mathbf{G}'-\mathbf{G}} & 0 \\ 0 & 0 & (1+\alpha)\delta_{\mathbf{G},\mathbf{G}'} \end{pmatrix} , \tag{5.29}$$

where

$$c_{\mathbf{G}} = \int_{\text{unit cell}} \mathrm{d}\mathbf{r}\ e^{-i\mathbf{G}\cdot\mathbf{r}}\ \cos 2\phi \tag{5.30}$$

$$s_{\mathbf{G}} = \int_{\text{unit cell}} \mathrm{d}\mathbf{r}\ e^{-i\mathbf{G}\cdot\mathbf{r}}\ \sin 2\phi\ . \tag{5.31}$$

If I define the first reciprocal lattice vector to be $\mathbf{G}_1$, then in the case of uniform helical advancement ($\phi = qz$), I find that $c_{\pm\mathbf{G}_1} = 1/2$, $\forall_{\mathbf{G}\neq\pm\mathbf{G}_1} c_{\mathbf{G}} = 0$, $s_{\pm\mathbf{G}_1} = \mp 1/2$ and $\forall_{\mathbf{G}\neq\pm\mathbf{G}_1} s_{\mathbf{G}} = 0$. Of course, in general things won't be so simple!

Given a definite form for $\underline{\underline{\epsilon}}^{-1}_{\mathbf{G}'-\mathbf{G}}$, I can substitute into equation (5.27) to find that for

normal incidence

$$\underline{\underline{A}}_{\mathbf{G}',\,\mathbf{G}} = b\,|\mathbf{k}+\mathbf{G}|\;|\mathbf{k}+\mathbf{G}'| \begin{pmatrix} \delta_{\mathbf{G},\mathbf{G}'} + \alpha c_{\mathbf{G}'-\mathbf{G}} & \alpha s_{\mathbf{G}'-\mathbf{G}} \\ \alpha s_{\mathbf{G}'-\mathbf{G}} & \delta_{\mathbf{G},\mathbf{G}'} - \alpha c_{\mathbf{G}'-\mathbf{G}} \end{pmatrix} . \tag{5.32}$$

Equations (5.24) and (5.32) can be rewritten in a dimensionless form. Since $\mathbf{G}$ and $\mathbf{k}$ both point along $\hat{z}$ for normal incidence, $|\mathbf{k}+\mathbf{G}| = k+G$. Given that $G = 2nq\hat{z}$, for $n$ integer, and using the previous definitions for $\tilde{k}$ and $\tilde{\omega}$, one obtains the result,

$$\tilde{\omega}^2 \mathbf{h}_{n'} = (\tilde{k}+n') \sum_n (\tilde{k}+n) \begin{pmatrix} \delta_{nn'} + \alpha c_{n'-n} & \alpha s_{n'-n} \\ \alpha s_{n'-n} & \delta_{nn'} - \alpha c_{n'-n} \end{pmatrix} \mathbf{h}_n . \tag{5.33}$$

### 5.2.2 1D periodic structure, oblique incidence

As in the previous subsection, I consider the simplification of equation (5.25) introduced by the presence of a 1-D periodic structure. I consider the periodicity to once again be along the $z$ axis, but unlike before, I allow $\mathbf{k}$ to point in any direction. A 1-D periodic structure has a coarse-grained cylindrical symmetry, which means that it looks the same, except for a phase, at any angle. Thus, the optical properties will be the same for any combination of $k_x$ and $k_y$ with the same overall magnitude $k_\rho = \sqrt{k_x^2 + k_y^2}$ to within the same phase as before. Thus, without loss of generality I write my $\mathbf{k} = k_\rho\hat{\rho} + k_z\hat{z}$ in cylindrical coordinates. Furthermore, the 1-D periodicity of the structure means that the overall magnitude of all fields must be the same under any arbitrary translation in the $xy$ plane. That implies that the magnetic field will only differ by a phase in the $xy$ plane. In conjunction with Bloch's theorem, that means I can write my field as a product of plane waves along $\hat{\rho}$ and $\hat{z}$ times a function periodic in $z$. In particular, I can write my previous expansion of the magnetic field, equation (5.17), in the particular form,

$$\mathbf{H}(\mathbf{r}) = \sum_G \sum_{\gamma=1}^{2} h_{(G\gamma)} \hat{e}_{(G\gamma)} e^{i[k_\rho\rho + (k_z+G)z]} . \tag{5.34}$$

I can easily show that

$$\nabla\cdot\mathbf{H}(\mathbf{r}) = i \sum_G \sum_{\gamma=1}^{2} h_{(G\gamma)} \left[k_\rho\hat{\rho} + (k_z+G)\,\hat{z}\right] \cdot \hat{e}_{(G\gamma)} e^{i[k_\rho\rho + (k_z+G)z]} . \tag{5.35}$$

One way to enforce the transversality constraint, equation (4.2) is to require each individual component of equation (5.35) to be transverse. Since each component is linearly independent, this is also the most general way available to ensure transversality. In this

case, I find that the particular form of $\mathbf{k}$ allows us to write equation (5.15) as

$$\forall_{G,\gamma}\ \left[k_\rho\hat{\rho} + (k_z + G)\,\hat{z}\right] \cdot \hat{e}_{(G\gamma)} = 0\ . \tag{5.36}$$

That condition puts two constraints on the coefficients of $\left\{\hat{e}_{(G\gamma)}\right\}$ for a given $G$. There is one constraint for each $\gamma$ imposed by the requirement that each $\hat{e}_{(G\gamma)}$ is a unit vector, and one more constraint from the orthogonality requirement given by equation (5.16). Thus, there is a total of five constraints and six components of $\hat{e}_{(G\gamma)}$ for each $G$. That allows us to choose one of the components arbitrarily. The simplest choice is to set $\hat{e}_{(G1)} = \hat{\theta}$, where $\hat{\theta}$ is the unit vector in the $xy$ plane orthogonal to $\hat{\rho}$. This choice trivially meets the condition on orthogonality given by equation (5.36). I also obtain as a result that

$$\hat{e}_{(G2)} = \frac{1}{\sqrt{k_\rho^2 + (k_z + G)^2}}\left[(k_z + G)\,\hat{\rho} - k_\rho\hat{z}\right]\ , \tag{5.37}$$

which is unique to within a factor of $\pm 1$ (although that is inevitable for a unit vector). Most importantly, I observe that unlike what I saw for normal incidence, each $\hat{e}_{(G\gamma)}$ will be different for each $G$ in general.

I can find a solution for $\underline{\underline{A}}_{n',\,n}$ in the reduced form

$$\tilde{\omega}^2\mathbf{h}_{n'} = \sum_n \underline{\underline{A}}_{n',\,n}\mathbf{h}_n\ , \tag{5.38}$$

which is equivalent to equation (5.24) in a dimensionless form. For simplicity, I calculate $\underline{\underline{A}}$ in Cartesian coordinates, which means $\mathbf{h}_n$ is a vector in Cartesian coordinates, and I am obliged to set $\tilde{\mathbf{k}} = \tilde{k}_\rho\hat{y} + \tilde{k}_z\hat{z}$. The result is

$$\underline{\underline{A}}_{n',\,n} = \begin{pmatrix} (\tilde{k}_z+n)(\tilde{k}_z+n')(\delta_{nn'}+\alpha c_{n'-n})+\tilde{k}_\rho^2(1+\alpha)\delta_{nn'} & (\tilde{k}_z+n)(\tilde{k}_z+n')\alpha s_{n'-n} & -\tilde{k}_\rho(\tilde{k}_z+n')\alpha s_{n'-n} \\ \alpha(\tilde{k}_z+n)(\tilde{k}_z+n')s_{n'-n} & (\tilde{k}_z+n)(\tilde{k}_z+n')(\delta_{nn'}-\alpha c_{n'-n}) & -\tilde{k}_\rho(\tilde{k}+n')(\delta_{nn'}-\alpha c_{n'-n}) \\ -\tilde{k}_\rho(\tilde{k}_z+n)\alpha s_{n'-n} & -\tilde{k}_\rho(\tilde{k}_z+n)(\delta_{nn'}-\alpha c_{n'-n}) & \tilde{k}_\rho^2(\delta_{nn'}-\alpha c_{n'-n}) \end{pmatrix}\ . \tag{5.39}$$

However, since $\mathbf{H}(\mathbf{r})$ must be transverse, I know that it really only has two degrees of freedom for each $G$, i.e., an $h_{(G1)}$ and an $h_{(G2)}$, i.e, $h_{(Gx)}$, $h_{(Gy)}$ and $h_{(Gz)}$ are interdependent. That implies that I can transform $\underline{\underline{A}}_{n',\,n}$ into a two-by-two matrix which I denote $\underline{\underline{A}}'_{n',\,n}$,

the solution for the analogue of equation (5.38),

$$\tilde{\omega}^2 \mathbf{h}'_{n'} = \sum_n \underline{\underline{A}}'_{n',\,n} \mathbf{h}'_n \,, \tag{5.40}$$

where $\mathbf{h}'_n = \begin{pmatrix} h_{(n1)} \\ h_{(n2)} \end{pmatrix}$. The resulting expression for $\underline{\underline{A}}'$ is

$$\underline{\underline{A}}'_{n',\,n} = \begin{pmatrix} (\tilde{k}_z+n)(\tilde{k}_z+n')(\delta_{nn'}+\alpha c_{n'-n})+\tilde{k}_\rho^2(1+\alpha)\delta_{nn'} & \alpha(\tilde{k}_z+n)(\tilde{k}_z+n')\sqrt{1+\left(\frac{\tilde{k}_\rho}{\tilde{k}_z+n}\right)^2}\, s_{n'-n} \\ \alpha(\tilde{k}_z+n)(\tilde{k}_z+n')\sqrt{1+\left(\frac{\tilde{k}_\rho}{\tilde{k}_z+n'}\right)^2}\, s_{n'-n} & (\tilde{k}_z+n)(\tilde{k}_z+n')(\delta_{nn'}+\alpha c_{n'-n})\sqrt{1+\left(\frac{\tilde{k}_\rho}{\tilde{k}_z+n}\right)^2}\sqrt{1+\left(\frac{\tilde{k}_\rho}{\tilde{k}_z+n'}\right)^2} \end{pmatrix} . \tag{5.41}$$

## 5.3 Simulation and Results

### 5.3.1 Simulation technique

In order to calculate the solutions to equation (5.33), I must rewrite it in a form amenable to computation. This requires us to choose a reasonable size for my plane-wave basis set, so that if $n$ and $n'$ range from $N$ to $-N$, I have a $2(2N+1)$ by $2(2N+1)$ matrix which links

$$\mathbf{h} = \left( \cdots h_{(-1,1)}\ h_{(0,1)}\ h_{(1,1)} \cdots h_{(-1,2)}\ h_{(0,2)} h_{(1,2)} \cdots \right)$$

and $\mathbf{h}'$, which is defined similarly. I can represent this linkage by the eigenvalue equation in the simple form

$$\tilde{\omega}^2 \mathbf{h}' = \underline{\underline{A}}\mathbf{h} \,, \tag{5.42}$$

where

$$\underline{\underline{A}} = \begin{pmatrix} \underline{\underline{A}}^{1,1} & \underline{\underline{A}}^{1,2} \\ \underline{\underline{A}}^{2,1} & \underline{\underline{A}}^{2,2} \end{pmatrix} , \tag{5.43}$$

and each individual $\underline{\underline{A}}^{\alpha,\beta}$ is a $2N+1$ by $2N+1$ array, calculated from the corresponding components of (5.33), e.g., $A^{1,1}_{n',n} = (\tilde{k}+n)(\tilde{k}+n')(\delta_{nn'}+\alpha c_{n'-n})$. I can show that $\underline{\underline{A}}$ is Hermitian, since $\left(A^{\beta,\alpha}_{n,n'}\right)^* = A^{\alpha,\beta}_{n',n}$, by inspection. Thus, all my eigenvalues are guaranteed to be real, as desired.

In order to solve my eigenvalue equation, I first construct the $\underline{\underline{A}}$ matrix, then diagonalise it. The construction of the matrix requires us to calculate the Fourier-coefficients,

which I do by first calculating the angle of the director for $2N+1$ evenly-spaced values of $z$ from equation (3.21) and the appropriate trigonometric identities for a fixed $r$, $\lambda$ and thus $\lambda_{yy}$. Then I populate the matrix using equations (5.33) and (5.43) for a given $\alpha$ and $\tilde{k}$.

Next, I diagonalise the matrix, using the procedure zheev in LAPACK, which computes all the eigenvalues and eigenvectors of a complex, double-precision Hermitian matrix [38]. Direct diagonalisation is clearly not the only way to solve the eigenvalue equation (5.42). Other methods, e.g., iterative eigensolvers, have been suggested and implemented as well [39]. However, direct diagonalisation can be performed for a matrix with a 32 plane-wave basis-set in less than 1 s per parameter set on a 266 MHz DEC alpha machine, which obviates any requirements for a lower-complexity algorithm.

### 5.3.2 1D periodic structure, normal incidence

#### Ideal helix

Here, I seek to reproduce the results of de Vries for an ideal helix at normal incidence, and develop an approach that will also apply to distorted helices and/or at oblique angles. There are only two harmonics, which allows us to write the values of $c_n$ and $s_n$ in particularly simple forms, namely, $c_{\pm 1} = 1/2$, $\forall_{|n|\neq 1}\ c_n = 0$, and $s_{\pm 1} = \mp i/2$, $\forall_{|n|\neq 1}\ s_n = 0$. These sine and cosine components link matrix elements which are a distance of $n$ apart. Since they vanish for $n > 1$, I only need to consider a small matrix in order to capture the structure of the matrix. I diagonalise this matrix in order to obtain the eigenvalues associated with my system. Since a system with no off-diagonal elements would be fully described for $N = 1$, I can easily guess that the ideal helix, with only the closest off-diagonal elements, is fully described by $N = 2$. That is confirmed by increasing $N$ in powers of two and comparing the results – to the accuracy of numerical algorithms, they are identical.

I construct the band structure by stepping through various values of $k$. Because of the periodicity of my lattice, $k$ is only unique modulo a reciprocal lattice vector, i.e., $\mathbf{k} = \mathbf{k}+\mathbf{G}$ in general. Also, since the $\underline{\underline{A}}$ matrix is Hermitian, I expect to find identical eigenvalues for $\mathbf{k}$ and $-\mathbf{k}$. In short, I only have to calculate the band structure for half of one Brillouin zone, and can trivially reproduce the rest as desired. In concrete terms, that means I only have to construct and diagonalise the $\underline{\underline{A}}$ matrix for approximately 20 values of the reduced $\tilde{k}$ between 0 and 0.5. I then plot the lowest $p$ eigenvalues versus $k$, and connect them into bands. The results of this procedure are depicted in figure 5.1. In terms of an extended zone scheme picture, there will be two bands associated with each $k$, two for each $k+2q$, two for each $k+4q$, etc. Two bands arise in general because photons in general

have two transverse polarisations (longitudinal polarisation is forbidden since they are massless). Thus, each pair of bands corresponds to two orthogonal polarisations. Based on the analysis of chapter 4, it is clear that the two polarisations will have distinctive behaviours, and that the pair with a gap at $k = q$ in figure 5.1 corresponds to circularly polarised light that rotates in the same sense as the helix outside the medium.

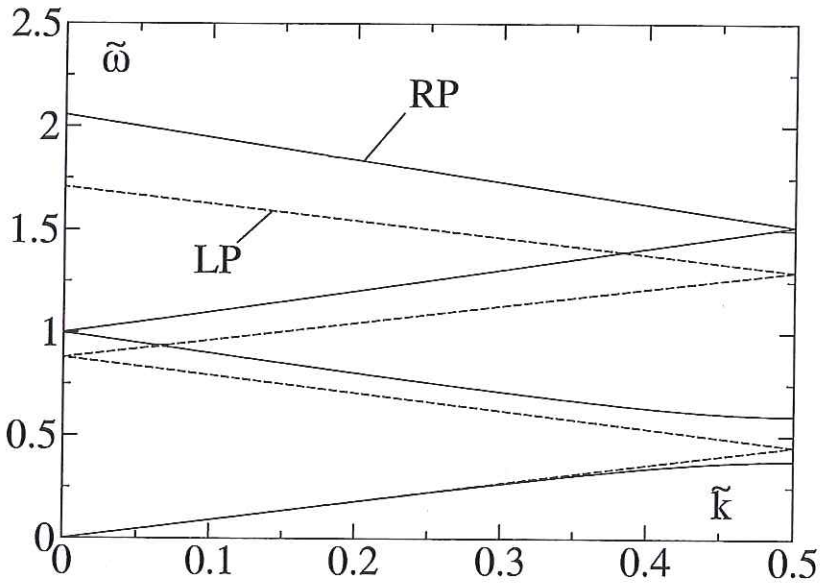


Figure 5.1: Dispersion relation from band-structure calculations, ($\tilde{\omega}$ versus $\tilde{k}$), for an ideal helix, with $\alpha = 0.18$. There is one gap for one polarisation, at $\tilde{k} = 1$, and no gap for the other polarisation.

However, it is important to note that figure 5.1 differs from figure 4.1 because the $\tilde{k}$, in chapter 4, henceforth referred to as $\tilde{k}'$, is in the rotating coordinate frame, while the $\tilde{k}$ in this chapter is in the stationary lab frame. Qualitatively, a wave with a $\tilde{k}'$ in the rotating frame is a coherent superposition of two waves with wavevectors $\tilde{k}' + 1/2$ and $\tilde{k}' - 1/2$ in the stationary frame. The gap that occurs at $\tilde{k}' = 0$ in figure 4.1 thus corresponds to a coherent superposition of states with $\tilde{k} = 1/2$ and $\tilde{k} = -1/2$. As can be seen in figure 5.1, there is a gap at $\tilde{k} = 1/2$, and by the reflection symmetry argument given above, there will also be one at $\tilde{k} = -1/2$. Similarly, a state with $\tilde{k}' = 1/2$ is a coherent superposition of the states at $\tilde{k} = 0$ and $\tilde{k} = 1$, which are the same since $\tilde{k}$ is only unique modulo a reciprocal lattice vector (which is one in reduced units). As can be seen by comparing the diagrams, the first and second frequencies match.

I also observe that there are no gaps for higher-order reflections. Since the dispersion relation in figure 4.1 has only one gap at $\tilde{k}' = 0$, this result is clearly predicted by de Vries' solution. The absence of higher order gaps does not hold in general, but only for normal incidence.

### Distorted Helix

The main case of interest is small deviations from ideal behaviour, a problem that is untractable in de Vries' approach but clearly amenable to band structure analysis. In the case of a cholesteric elastomer, a physical example of small deviations from ideality corresponds to a moderate $x$-strain perpendicular to the pitch axis. My procedure for numerical solution of the problem is as follows. First, I choose a particular value for $r$ and a value for $\lambda$ greater than but close to one. I then numerically minimise the coarse-grained energy $F'(\lambda, \lambda_{yy}, r)$ with respect to $\lambda_{yy}$ to obtain its value. I can then use equation (3.21) to calculate the critical values for the angles, and equation (3.22) to choose those that correspond to minima in the free energy. Trigonometric identities can be used to obtain the corresponding values of $\cos 2\phi$ and $\sin 2\phi$. A fast fourier transform will then give us the appropriate values of $c_n$ and $s_n$. It is simple to guess, by analogy with perturbation theory in quantum mechanics, that small deviations away from ideality will lead to small values for $c_n$ and $s_n$ where $|n| \neq 1$. Furthermore, I expect that these small values will scale as power laws in the small parameter of the problem, the strain $e \equiv \lambda - 1$. The scaling of these coefficients is given by

$$s_n = \begin{cases} 0 & \text{if } n = 0, \\ \mp\frac{i}{2}\left[1 - \mathcal{O}(e^2)\right] & \text{if } n = \pm 1, \\ \mp i\, \mathcal{O}(e^{n-1}) & \text{otherwise,} \end{cases} \tag{5.44}$$

and

$$c_n = \begin{cases} \mathcal{O}(e) & \text{if } n = 0, \\ \frac{1}{2}\left[1 - \mathcal{O}(e^2)\right] & \text{if } n = \pm 1, \\ \mathcal{O}(e^{n-1}) & \text{otherwise,} \end{cases} \tag{5.45}$$

where terms of the form $\mathcal{O}(x)$ are interpreted to mean a quantity given by the product of $x$ and a real number of order unity.

The variation of the Fourier components of $\sin 2\phi(z)$ and $\cos 2\phi(z)$ is illustrated in figures 5.2 and 5.3 for a cholesteric elastomer under an $x$-strain of $\lambda$. A similar pattern can be seen in the case of a liquid cholesteric under an external electric or magnetic field, as shown in figures 5.4 and 5.5. I can calculate the scaling behaviour for $c_n$ and $s_n$ in an external field by transforming the scaling laws given in equations (5.44) and (5.45), and effecting the transformation $e \to (H/H_c)^2$, for $H \leq H_c$.

Given the values of $s_n$ and $c_n$ at a given $r$ and $\lambda$, I can calculate the band-structure

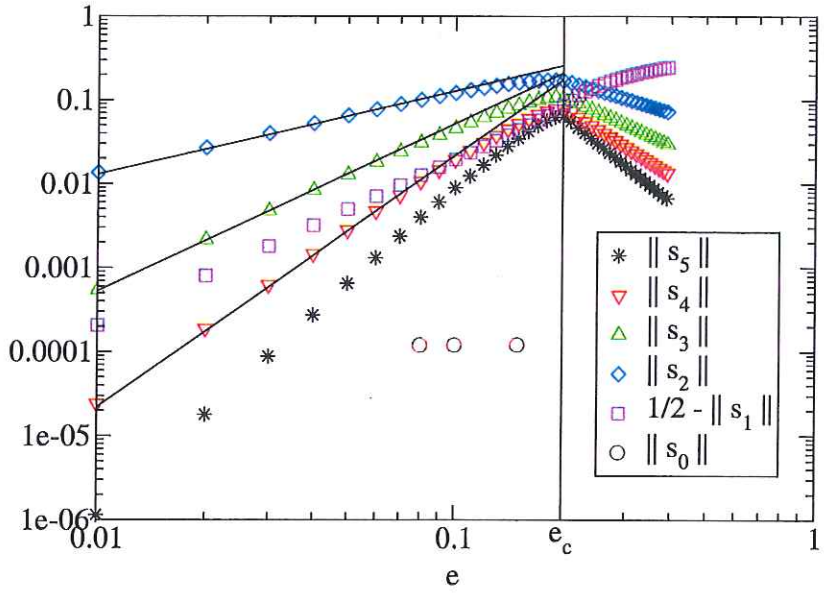


Figure 5.2: Values for various $s_n$ in a cholesteric elastomer experiencing a uniaxial $x$-strain.

numerically, just as I did in the de Vries case, figure 5.1. I illustrate two examples: $\lambda = 1.1 < \lambda_c$ in figure 5.6 and $\lambda = 1.3 > \lambda_c$ in figure 5.7, both at $r = 1.9$. In figure 5.6, the sample is stretched by less than the critical strain, which is given by $\lambda_c \approx r^{2/7} \approx 1.19$ [23]. Stretching leads to coarsening of the helix which in turn gives rise to new gaps at higher orders at the Brillouin zone boundaries, particularly for the polarisation that rotates along with the helix. But there are also smaller gaps that arise for the opposite handedness even before we reach the critical strain $e_c$. We can explain this phenomenon by considering that, in the uniformly rotating frame in which our original $E_\xi$ and $E_\eta$ live, there are, in effect, rotations of $\mathbf{n}$ both forwards and backwards that arise from deviations of $\phi'(z)$ from the unperturbed constant value of $q$ (see figures 2.3 and 3.2). The size and scaling of these gaps is discussed below. The position of these gaps is constant to the first order in my reduced notation, but actually varies in a physical system. In particular, since a uniaxial strain of $\lambda$ along $x$ leads to a contraction $\lambda_{zz} = \lambda^{-2/7}$, my wavevector $q = q_0\lambda^{2/7}$. Since the Brillouin zone boundaries occur at integer multiples of $q$, they will shift to higher values. Physically, that will correspond to reflections at higher frequencies. Since $\tilde{\omega} = \omega/2cq\sqrt{b}$, a constant $\tilde{\omega}$ corresponds to a physical $\omega$ that also scales like $\omega = \omega_0\lambda^{2/7}$, where $\omega_0$ denotes a frequency of interest at zero strain. Thus, these shifts are scaled away in figures 5.6 and 5.7. Experimental evidence for the predicted shift in the band gaps toward the ultraviolet has been seen in two sets of experiments.

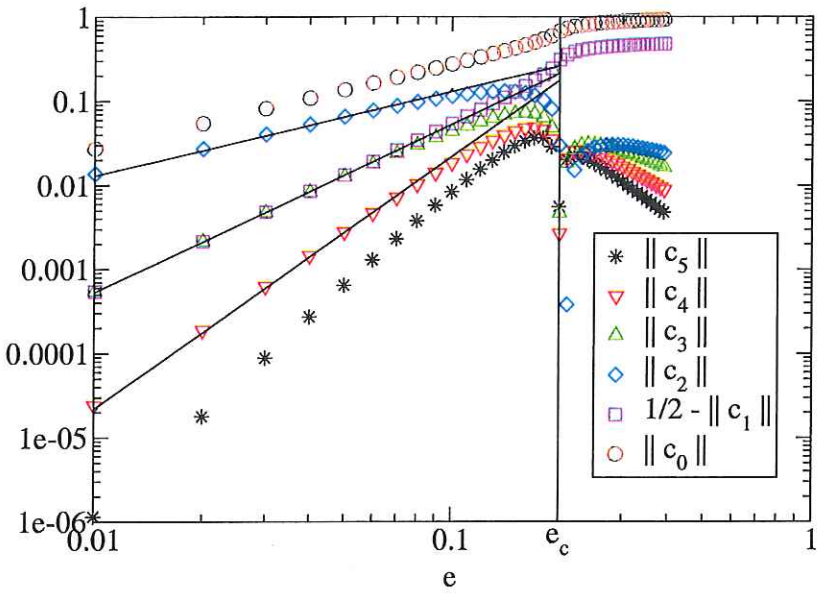


Figure 5.3: Values for various $c_n$ in a cholesteric elastomer experiencing uniaxial stretching

First, there is a change in the colour of cholesteric monodomain rubbers upon stretching [22, 33]. Furthermore, there are changes in the colour of the lasing mode as stretching proceeds [6].

In figure 5.7, the sample is stretched beyond the critical strain. This gives rise to a qualitative change in the behaviour of the director, $\phi(z)$ (see figure 3.2), and thus a qualitative change in the band structure. The most important effect is the elimination of the persistent bias toward rotation in one direction present at smaller strains; now, the director rotates periodically, swinging almost equally in both directions. Removing this bias means that there should be little difference between the optical properties of left- and right-circularly polarised light. Furthermore, the magnitude of this difference will decrease with increasing $e$. As a result, the circular dichroism of the material should disappear, and the eigenmodes of light inside the stretched cholesteric medium should be linearly polarised. Also, I note that the scaling behaviour of $\lambda_{zz}$ crosses over from the non-classical $\lambda^{-2/7}$ response to a $\lambda^{-1/2}$ response, the classical exponent predicted for isotropic elastomers (e.g., rubbers without nematic ordering). That in turn implies that the frequencies reflected increase more quickly with strain, i.e., $\omega = \omega_0 \lambda^{1/2}$, but the range decreases in width, owing to the decreasing magnitude of the oscillations about $\phi = 0$.

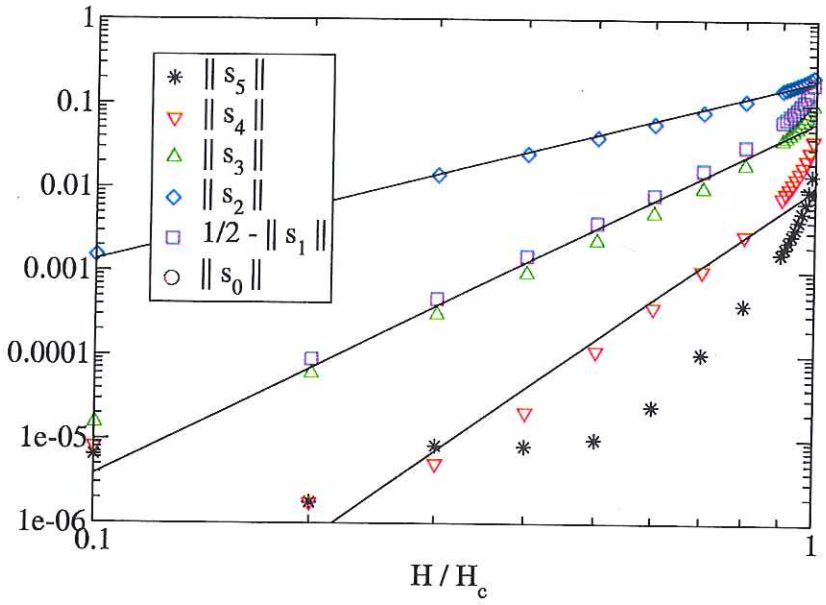


Figure 5.4: Values for various $s_n$ in a liquid cholesteric subjected to an external uniform electric or magnetic field. Note that all $s_n$ go abruptly to zero for fields $H$ greater than the critical field $H_c$ (unlike figure 5.2).

### Perturbation theory of gap scaling

I can apply second-order degenerate perturbation theory to calculate the approximate size and scaling of the band gaps. In electronic structure theory, one can take an approach analogous to my photonic band structures, and construct an $A_{ij}$ that satisfies the Schrödinger equation, where $\psi$ is expanded in a plane-wave basis set, and it is assumed to be a scalar quantity (thereby ignoring spin). I then identify two degenerate states, $n$ and $n'$, and then construct the reduced matrix

$$\underline{\underline{D}} = \begin{pmatrix} A_{nn} & A_{nn'} \\ A_{n'n} & A_{n'n'} \end{pmatrix} . \tag{5.46}$$

This procedure should give an accurate answer provided that the off-diagonal elements are relatively small. In the case of light normally incident upon a distorted cholesteric helix, I can surmise from equation (5.33) that $A_{nn} = (\tilde{k}+n)^2(1+\alpha c_0)$ and $A_{n'n'} = (\tilde{k}+n')^2(1-\alpha c_0)$. Also, the off-diagonal elements will be $A_{n'n} = (A_{nn'})^* = \alpha(\tilde{k}+n)(\tilde{k}+n')s_{n'-n}$ (since $\underline{\underline{A}}$ is Hermitian). Since I am interested in splitting between nearly degenerate energy levels, I must have $A_{nn} \approx A_{n'n'}$, which is satisfied when $\left|\tilde{k}+n\right| = \left|\tilde{k}+n'\right|$. For the interesting case where $n \neq n'$, that is equivalent to saying $\tilde{k} = -(n+n')/2$. Substituting back into

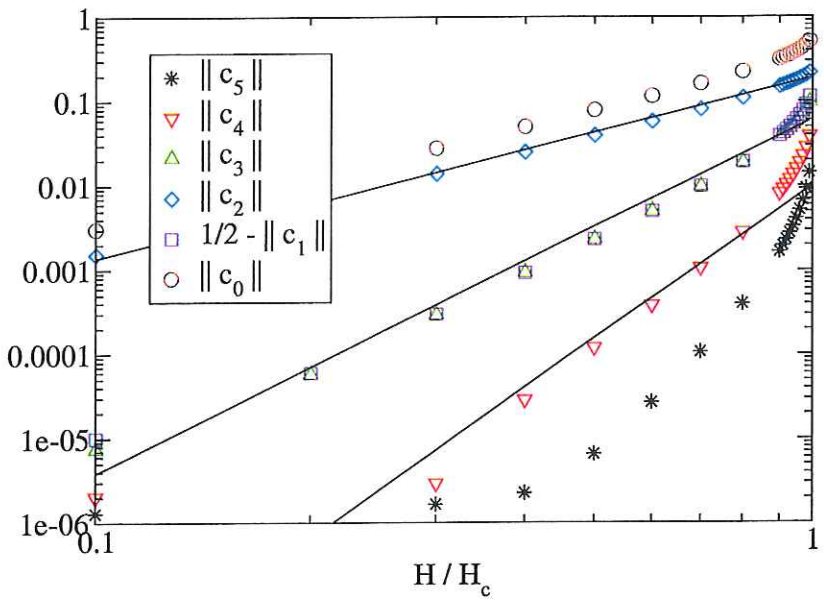


Figure 5.5: Values for various $c_n$ in a liquid cholesteric subjected to an external uniform electric or magnetic field. Note that all $c_n$ except for $c_0$ go abruptly to zero for fields $H$ greater than the critical field $H_c$ (unlike figure 5.3).

equation (5.46), I obtain

$$\underline{\underline{D}} = \begin{pmatrix} \frac{(n-n')^2}{4}(1+\alpha c_0) & -\alpha\frac{(n-n')^2}{4}s_{n'-n} \\ -\alpha\frac{(n-n')^2}{4}s_{n-n'} & \frac{(n-n')^2}{4}(1-\alpha c_0) \end{pmatrix} \tag{5.47}$$

From equation (5.47), I obtain a pair of eigenvalues corresponding to the two new frequencies resulting from the splitting of the degeneracy. In a dimensionless form, they are given by the expression

$$\tilde{\omega}^2 = \left(\frac{\delta n}{2}\right)^2 \left[1 \pm \alpha\sqrt{c_0^2 - s_{\delta n}^2}\right] , \tag{5.48}$$

where $\delta n = n - n'$. For an undistorted helix, $c_0 = 0$, $s_{-1} = -s_1 = i/2$, and $\forall_{|n|\neq 1}\, s_n = 0$, which gives us the result $\tilde{\omega}^2 = \frac{1}{4}\left[1 \pm \frac{1}{2}\alpha\right]$, which for a small value of $\alpha$ corresponds to a splitting $\delta\tilde{\omega} = \alpha/4$, a linear dependence on the reduced dielectric anisotropy, as was originally predicted by de Vries. All other gaps will vanish since $\forall_{|\delta n|\neq 1} s_{\delta n} = 0$.

For a slightly distorted helix, given the scaling relations I found before, I can generalise from equation (5.48) to calculate the size of the gap for any order. Given that $c_0 = 0$, I obtain $\delta\tilde{\omega} = (\delta n/2)\alpha\,|s_{\delta n}|$, which thus scales like $\delta\tilde{\omega} \approx (\delta n/2)\alpha e^{\delta n - 1}$. Since I already have the scaling relations for the Fourier-coefficients, I immediately know how the gaps should

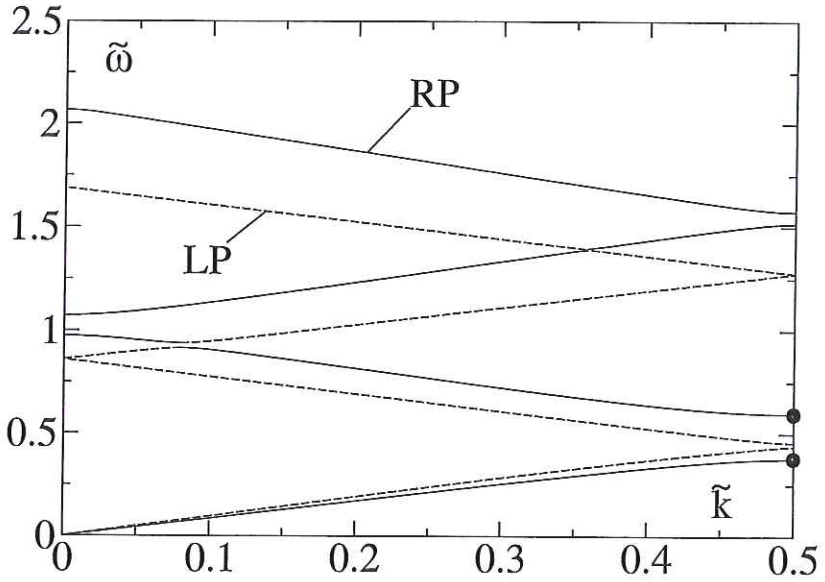


Figure 5.6: Band structure for a cholesteric elastomer at a strain of $\lambda = 1.1$, with anisotropy $r = 1.9$. The dots indicate the position of the only band gap present in the ideal helix, for comparison.

behave as well. These predictions are confirmed qualitatively by inspection of the figures; however the results are not exact.

A more precise approach calls for us to account for the vector nature of the photons. Unlike most electronic structure calculations, the photonic calculations require us to account for the polarisation for accuracy. Physically, this occurs because the inverse dielectric tensor represents an effective potential for the photons. Deviations of the dielectric tensor from the unit tensor times a constant represent the magnitude of the difference of the effective potential acting upon different polarisations. In my reduced units, this magnitude is naturally given by $\alpha$ and is therefore not negligible.

The vectorised approach requires us to include a total of sixteen elements, arranged in two levels of two-by-two matrices. The inner matrices each consist of elements for a given $\gamma$ and $\gamma'$ for all combinations of $n$ and $n'$. The outer matrices obvious vary $\gamma$ and $\gamma'$, then. The result looks like the following:

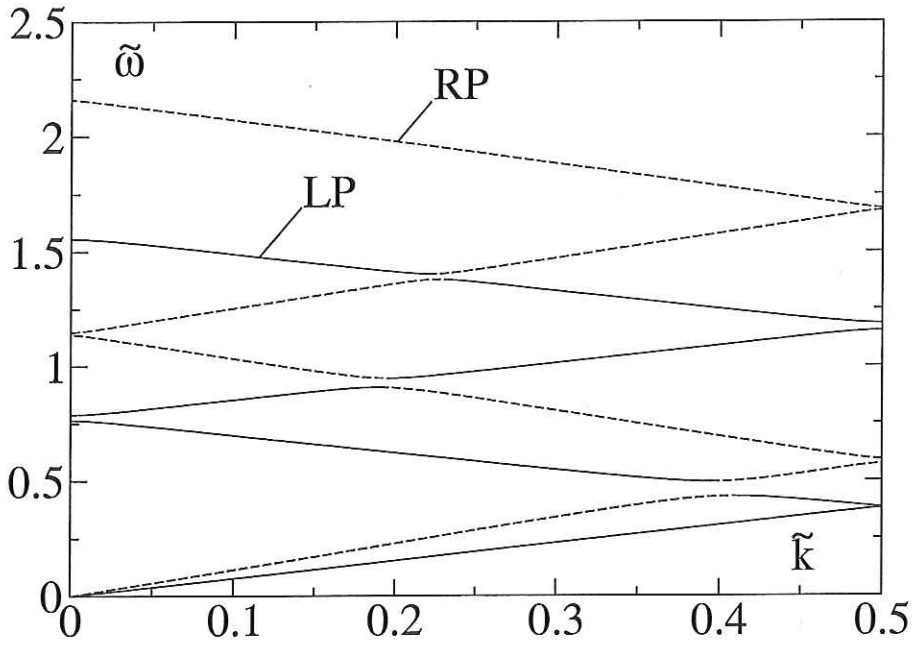


Figure 5.7: Band structure for a cholesteric elastomer at a strain of $\lambda = 1.3$, with anisotropy $r = 1.9$.

$$\underline{\underline{D}} = \begin{pmatrix} (k+n)^2(1+\alpha c_0) & \alpha(k+n)(k+n')c_{n'-n} & 0 & \alpha(k+n)(k+n')s_{n'-n} \\ \alpha(k+n)(k+n')c_{n-n'} & (k+n')^2(1+\alpha c_0) & \alpha(k+n)(k+n')s_{n-n'} & 0 \\ 0 & \alpha(k+n)(k+n')s_{n'-n} & (k+n)^2(1-\alpha c_0) & -\alpha(k+n)(k+n')c_{n'-n} \\ \alpha(k+n)(k+n')s_{n-n'} & 0 & -\alpha(k+n)(k+n')c_{n-n'} & (k+n')^2(1-\alpha c_0) \end{pmatrix} . \quad (5.49)$$

Given that $\tilde{k} = -(n+n')/2$, I obtain the eigenvalues

$$\tilde{\omega}^2 = \left(\frac{\delta n}{2}\right)^2 \left[1 \pm \alpha\left(c_{\delta n} \pm \sqrt{c_0^2 - s_{\delta n}^2}\right)\right] . \quad (5.50)$$

This now gives us four eigenvalues at the Brillouin zone boundary, split from a quadruple degeneracy of two dispersion relations with two polarisations each meeting at one point in $\tilde{k}$. Clearly in the undistorted case, I will obtain $\tilde{\omega}^2 = \frac{1}{4}\left[1 \pm \alpha\left(\frac{1}{2} \pm \frac{1}{2}\right)\right]$. I interpret this answer as corresponding to two eigenmodes rotating with the helix that are split such that $\tilde{\omega}^2 = \frac{1}{4}[1 \pm \alpha]$, and two eigenmodes rotating against the helix that are unsplit so that both $\tilde{\omega}^2 = \frac{1}{4}$. I obtain the same result through numerical diagonalisation of my $\underline{\underline{A}}$ matrix for $N \geq 2$. For a distorted helix, given that $c_0 = fe$ and that $s_1 = i(1/2 - ge^2)$

and $c_1 = 1/2 - he^2$, I expect that

$$\tilde{\omega}^2 = \frac{1}{4}\left[1 \pm \alpha\left(1/2 - he^2 \pm \sqrt{(fe)^2 + (1/2 - ge^2)^2}\right)\right], \tag{5.51}$$

which corresponds to a large gap for the polarisation that rotates along with the helix, given by $\tilde{\omega}^2 = (1/4)\left[1 \pm \alpha\left(1 + (f^2 - g - h)\,\delta^2\right)\right]$, and a small gap for the opposite helicity, given by $\tilde{\omega}^2 \approx (1/4)\left[1 \pm \alpha(g - h - f^2)\delta^2\right]$, corresponding to a gap of width $\delta\omega = (1/2)\alpha\left(g - h - f^2\right)\delta^2$. Since $g - h - f^2$ is non-vanishing in general, I expect that both band gaps will be non-zero. These results correspond qualitatively to the scaling behaviour observed in figures 5.8 and 5.9. Since the smaller gap is centered about the same value of $\tilde{\omega}^2$ as the larger gap, I am led to predict a *full* photonic band gap for a distorted helix at normal incidence, i.e., I expect that normally incident light of *any* polarisation with frequencies within the band-gap will be totally reflected.

I will now attempt to extend the theory for splitting at the first Brillouin zone boundary to higher orders. An important factor affects these anti-crossings, namely, the gradual separation of the dispersion relations for eigenmodes that tend to point along $\epsilon_\perp$, and eigenmodes that tend to point along $\epsilon_\parallel$. Since these two sets of eigenmodes experience a different effective refractive index, they have different slopes which gives rise to two meeting points that gradually separate as I go to higher bands (corresponding to higher Brillouin zones in an extended-zone scheme). Furthermore, some of the higher crossings can take place away from the zone boundaries; however, those effects require mixing between two nearly orthogonal modes and are usually small. In practical terms, that means that rather than four-wave splitting, I must instead consider two-wave splitting at higher Brillouin-zone boundaries. Fortunately, that is relatively easy. My matrix becomes

$$\underline{\underline{D}} = \begin{pmatrix} \left(\frac{\delta n}{2}\right)^2(1 \pm \alpha c_0) & \mp\alpha\left(\frac{\delta n}{2}\right)^2 s_{\delta n} \\ \mp\alpha\left(\frac{\delta n}{2}\right)^2 s^*_{\delta n} & \left(\frac{\delta n}{2}\right)^2(1 \pm \alpha c_0) \end{pmatrix} \tag{5.52}$$

That gives rise to two pairs of eigenvalues: $\tilde{\omega}^2 = \left(\frac{\delta n}{2}\right)^2\left[1 - \alpha\left(c_0 \pm i s_{\delta n}\right)\right]$ and $\tilde{\omega}^2 = \left(\frac{\delta n}{2}\right)^2\left[1 + \alpha\left(c_0 \pm i s_{\delta n}\right)\right]$, corresponding to a band gap of magnitude $\delta\omega \approx (\delta n/2)\alpha\,|s_{\delta n}|$.

### Scaling of band gaps with mechanical strain

Of experimental interest is the *in vacuo* wavelength, $\Lambda$, of the light corresponding to a given $\tilde{\omega}$ on the CE dispersion relation, particularly at the gaps. The previous definitions give $\Lambda = p_0/(\tilde{\omega}\sqrt{b}\lambda^{2/7})$. Pitches $p_0$ typically give a band in the visible so the initial wavelengths are $\Lambda_0 = p_0/\sqrt{b} \sim 500\text{nm}$ at $\tilde{\omega} = 1/2$ and $\lambda = 1$, which allows us to write $\Lambda = \Lambda_0/(2\tilde{\omega}\lambda^{2/7})$. Likewise the first order de Vries gap is given by $\Delta\Lambda \approx \Lambda_0/\lambda^{2/7}\alpha$. The

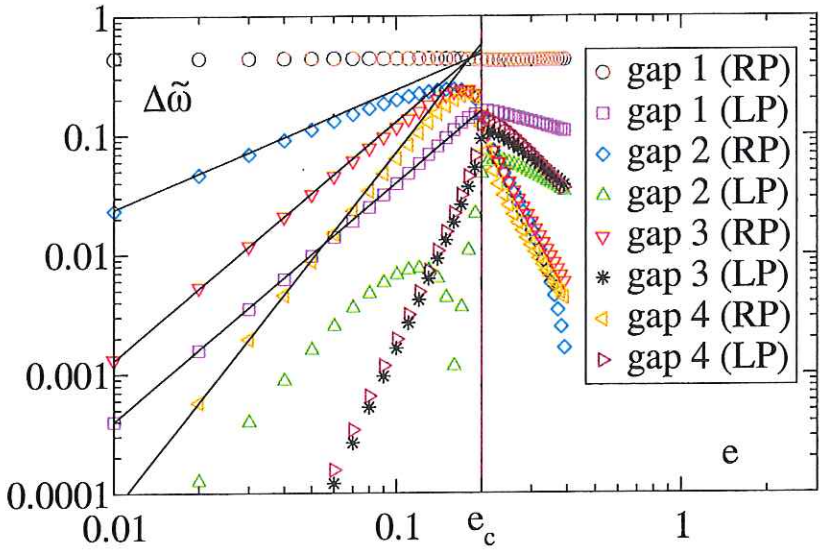


Figure 5.8: Scaling of various gap sizes as a function of the strain, $e$.

higher order gaps of the same polarisation will have widths of $\Delta\Lambda_n \approx C\Lambda_0 e^{n-1}/(n\lambda^{2/7})$, where $C$ is a pre-factor of order unity that will depend on $r$ and $\alpha$. For example, the second order gap in a rubber with $r = 1.9$, $\alpha = 0.43$, and $e = 0.1$, the gap will be $\Delta\Lambda_2 \approx 0.045\Lambda_0$. For $\Lambda_0 \approx 800$nm, that implies a stop band for the light with a circular polarisation of the same sense as the helix will be observed for $\Lambda = 362$ nm to $\Lambda = 398$ nm.

### 5.3.3 1D periodic structure, oblique incidence

In figures 5.10, 5.11 and 5.12, I show full band structure calculated using my methodology for arbitrary angles of propagation (i.e., arbitrary $\mathbf{k}$ inside the cholesteric medium). These results were obtained by diagonalisation of the matrix in equation (5.41), which is specifically suited to the case of light propagating at arbitrary angles in one-dimensionally periodic structures, such as chiral nematics. Thus in addition to the case of cholesterics discussed in this thesis, the same equation may be used to study materials such as piezoelectrics. In my photonic band structures, I imitate the style of electronic band structures by traversing a range of $\mathbf{k}$ values so that I have an idea of how $\omega$ can vary. The rules are that I increase or decrease each component of $\mathbf{k}$ (in this case, there are only two, $k_\rho$ and $k_z$) according to a specified rule until I hit a zone boundary then "reflect back" or start using a different rule. The most efficient way of traversing the space of a Brillouin zone is usually called the "irreducible Brillouin zone." However, the lack of periodicity along $\rho$ (perpendicular to the pitch axis), means that each $k_\rho$ is unique, and thus, I'll never hit a boundary in that direction. However, I can make up for this deficiency by

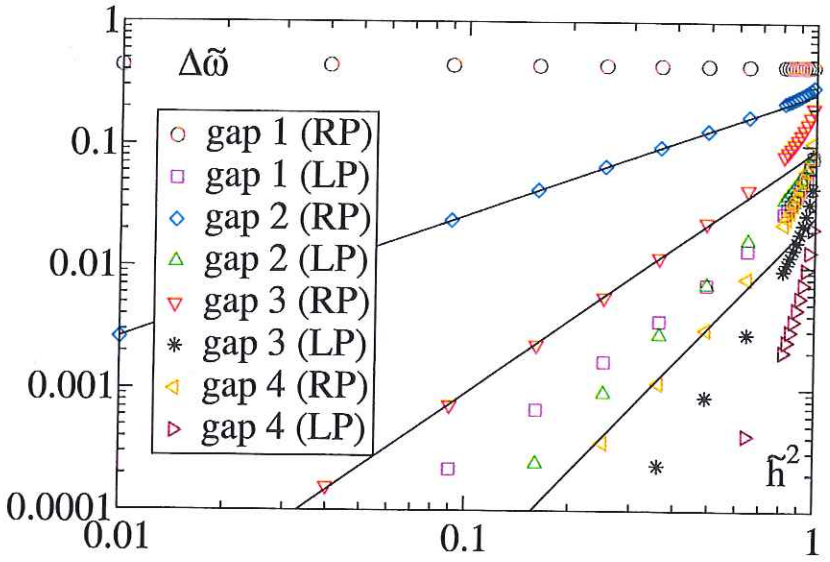


Figure 5.9: Scaling of various gap sizes as a function of the reduced external field, $(H/H_c)^2$. Note how the scaling corresponds to that seen in figure 5.8

the fact that the lowest bands (corresponding to visible light when the pitch is about one optical wavelength) will have a natural limit on $k_\rho$ since *in vacuo*, $\omega \geq c\,|k_\rho|$, and in the cholesteric medium, $\tilde{\omega} \geq (1-\alpha)|\tilde{k}_\rho|$. Qualitatively, these results mean low frequencies must have a correspondingly low $k_\rho$. Thus, practically, this issue does not present a great problem.

Starting from the left, the first rule is to increase $k_z$ only, which corresponds to the band structure for normal incidence. I can verify that the first parts of figures 5.10, 5.11 and 5.12 are identical to figures 5.1, 5.6 and 5.7, respectively. Once I reach the first zone boundary and observe the familiar gaps, I then begin to increase $k_\rho$, which corresponds to a gradual tilt away from propagation normal to the director, until the two components are equal. At that point, the **k** will correspond to 45° propagation within the medium. I then gradually decrease the magnitude of **k**, without changing the direction. Here, one can observe hints of at least one Bragg reflection for *both* senses of polarisation, even for an ideal helix. More reflections would be visible if I were to sweep over a broader range of $k_\rho$ values. In the fourth and final portion of the diagram, I look at the case of $k_z = 0$, corresponding to 90° propagation, along a direction perpendicular to the pitch axis (taken to be along $\hat{y}$ for simplicity).

For figure 5.10, the ideal helix, I note the following features. First, there is a gap for light propagating at 45° for both polarisations. This obviously contrasts strongly with the normally incident case, in which only one polarisation experiences a gap, and is reminiscent of the opening of gaps at normal incidence upon distortion. In both cases,

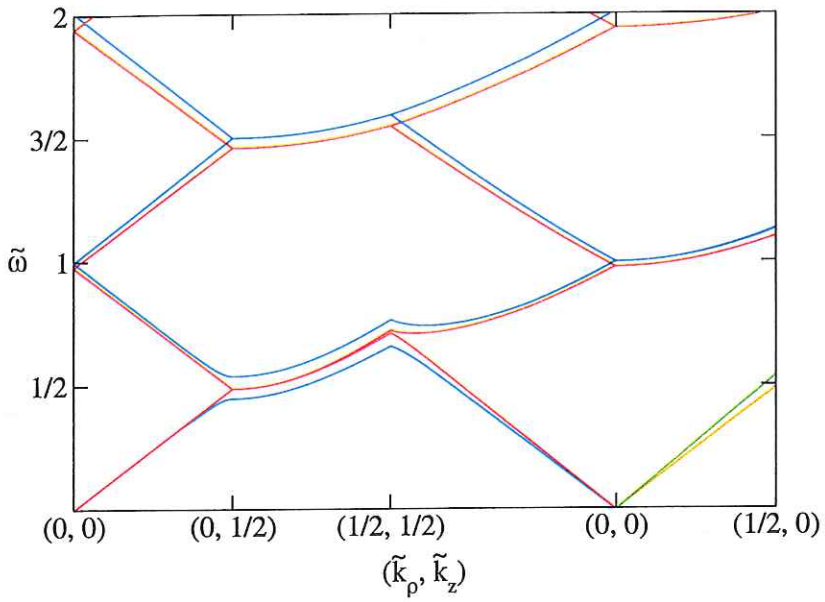


Figure 5.10: Full dispersion relation at several directions of propagation in an ideal helix: (1) normal, (2) increasingly away from normal up to 45°, (3) 45° propagation for a decreasing magnitude of $k$, and (4) 90°

I observe the same sort of behaviour in the sense that a large, first-order gap for the polarisation that rotates with the helix remains, while a smaller gap opens up as I move away from normal incidence with constant $k$. However, there is a difference between the two as regards the gap scaling. For small angles away from normal incidence, I observe that the smaller gap scales as $\theta^2$ while the larger gap goes as $\alpha\left(1/2 - \mathcal{O}\left(\theta^2\right)\right)$. Conversely, small stretching of a cholesteric rubber makes for a smaller gap that scales as $e$, along with a larger gap that scales as $\alpha\left(1/2 - \mathcal{O}\left(e^2\right)\right)$. Also, the direction of the dispersion relations is such that the frequencies trend upwards as the angle of incidence increases. Incidentally, that may provide an explanation for the success of lasing on the band-edge of cholesterics [5]. To wit, a lasing mode just above the lower frequency allowed at normal incidence will be forbidden above a critical angle. As one gets closer to the bottom of the upper part of the dispersion curve, the smaller the critical angle becomes. For a small enough critical angle, light will essentially be forced to propagate straight through the cholesteric medium, which will clearly assist in the collimation of light, and the focusing of the energy of an emitted – more of the pumping power is utilised.

Also, the eigenmodes of a beam propagating at an angle 90° from normal will differ enormously from what was discussed previously for normal incidence. Out of the two lowest eigenmodes, one has a dispersion relation given by $\tilde{\omega}^2 = (1+\alpha)\tilde{k}_\rho^2$, and a linear polarisation along $\hat{x}$ (assuming $\mathbf{k} = 2q\tilde{k}_\rho\hat{y}$). This polarisation corresponds to an $\mathbf{E}$ which

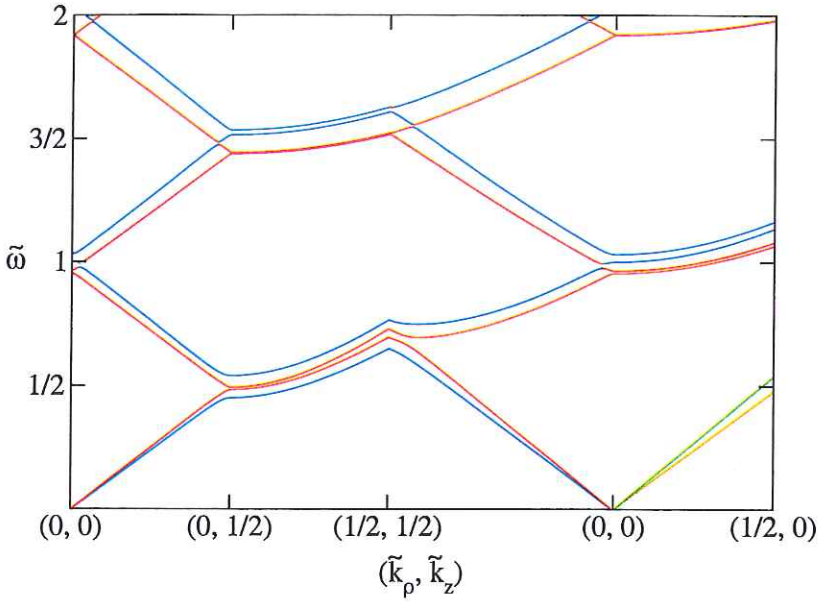


Figure 5.11: Full dispersion relation at multiple angles for a helix distorted by a strain $e = 1.1 < e_c$ $(r = 1.9)$.

points wholly along $\hat{z}$, the direction of unvarying dielectric constant. The other polarisation points all over space in a highly non-trivial manner, as a periodic function of $y$ and $z$. This periodic variation costs a larger amount of energy than pointing along a constant direction. Nonetheless, since this polarisation is able to take advantage of being able to direct its $\mathbf{E}$ along a higher dielectric constant direction than the trivial polarisation, it is lower in energy despite its twisting and turning. An illustration of how its direction and magnitude (in spherical coordinates) depend on $y$ and $z$ is given in figures 5.13-5.15. Thus in the last sector of 90° propagation shown in figures 5.10-5.12 (where $(0,0) \rightarrow (1,0)$), the lowest linear dispersion is the non-trivial mode, and the higher linear dispersion in the trivial mode.

Furthermore, there are multiple Bragg reflections. While that is generally expected within the context of periodic band structures, that is surprising for a cholesteric, which only has one gap at normal incidence. These reflections are like the elastic scattering of an electron in a crystal, and so they will take place when the incoming and outgoing wavevectors are the same modulo a reciprocal lattice vector, i.e., when $\mathbf{k}^2 = (\mathbf{k} + \mathbf{G})^2$. This condition is equivalent to $2\mathbf{k} \cdot \mathbf{G} = \mathbf{G}^2$, and yields $\tilde{k}_z = \pm n/2$ for $n$ integer. At a given angle of propagation $\theta > 0$ such that $\tilde{k}_\rho = \tilde{k} \sin\theta$ and $\tilde{k}_z = \tilde{k} \cos\theta$, the reflections will take place at $\tilde{k} = \pm n/(2\cos\theta)$.

However, the data in figures 5.10- 5.12 is not directly applicable to experiment. That is because at an interface between the cholesteric medium and a homogeneous medium,

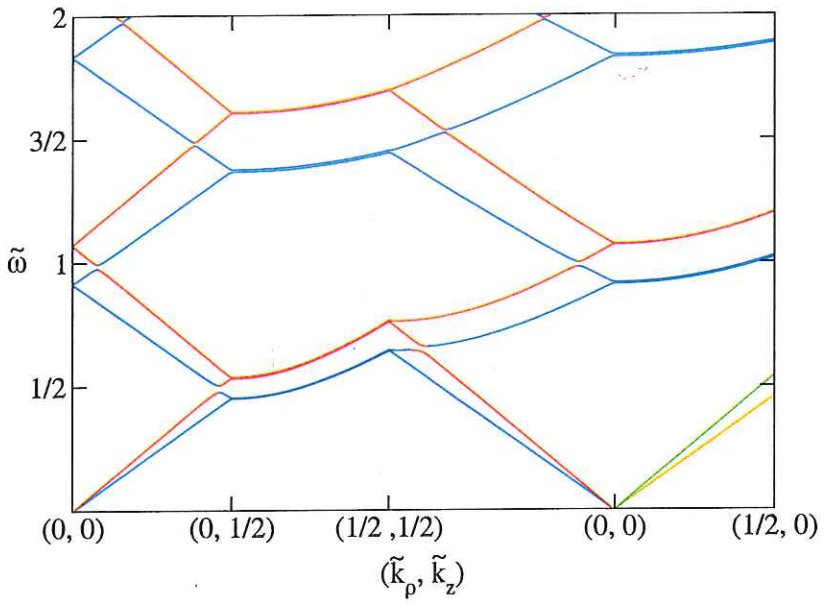


Figure 5.12: Full dispersion relation at multiple angles for a helix distorted by a strain $e = 1.3 > e_c$ $(r = 1.9)$.

not all components of **k** are conserved. Based on the previous arguments about boundary conditions given in chapter 4, it can be shown that while $k_\rho$ will be conserved across the boundary, $k_z$ will not be (Snell's law). Nonetheless, the information in the previous curves can be processed to yield experimentally useful data. One approach is based on the work of Yoel Fink and colleagues [40]. If the value for $\tilde{k}_\rho$ is fixed, then sweeping across all the unique values of $\tilde{k}_z$ will yield all of the allowed frequencies for that $\tilde{k}_\rho$. Repeating over a number of $\tilde{k}_\rho$ yields a diagram that has "bubbles" corresponding to forbidden combinations of $\tilde{k}_\rho$ and $\tilde{\omega}$, as shown in figure 5.16. Thus, at least one polarisation of light in the shaded regions will be transmitted, while the light in the bubbles will be wholly reflected for all polarisations. If one fixes the slope of the relation between $\tilde{k}$ and $\tilde{\omega}$, it will correspond to fixing the angle of incidence outside the medium while varying the frequency of the incident light. In this case, one finds total reflections spaced at integer multiples of a fundamental frequencies at angles ranging from 22.5° to 67.5° incidence. Also, the frequencies at which the reflections take place increase as the angle away from normal incidence is increased, as is predicted by the previous considerations for elastic scattering, and observed experimentally by Takezoe *et al.* [41].

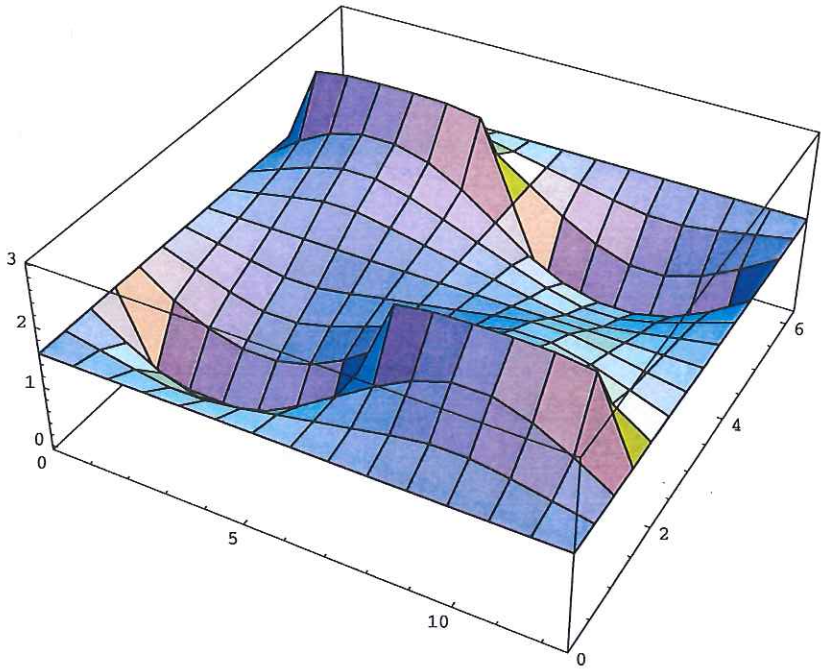


Figure 5.13: A plot of the angle $\theta$ versus the $y$ and $z$ coordinates for t he first eigenmode ($y$ axis is on the bottom).

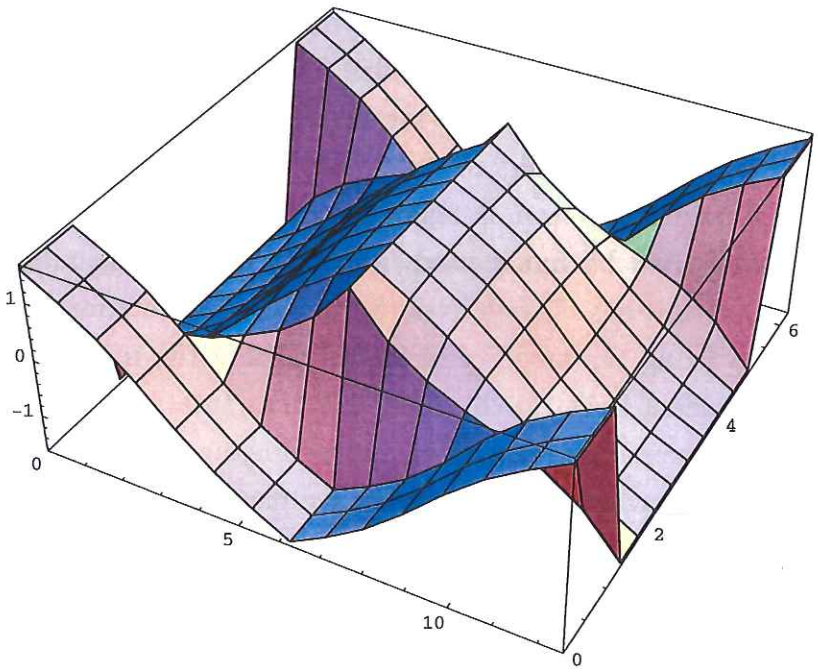


Figure 5.14: A plot of the angle $\phi$ versus $y$ and $z$ for the first eigenmode.

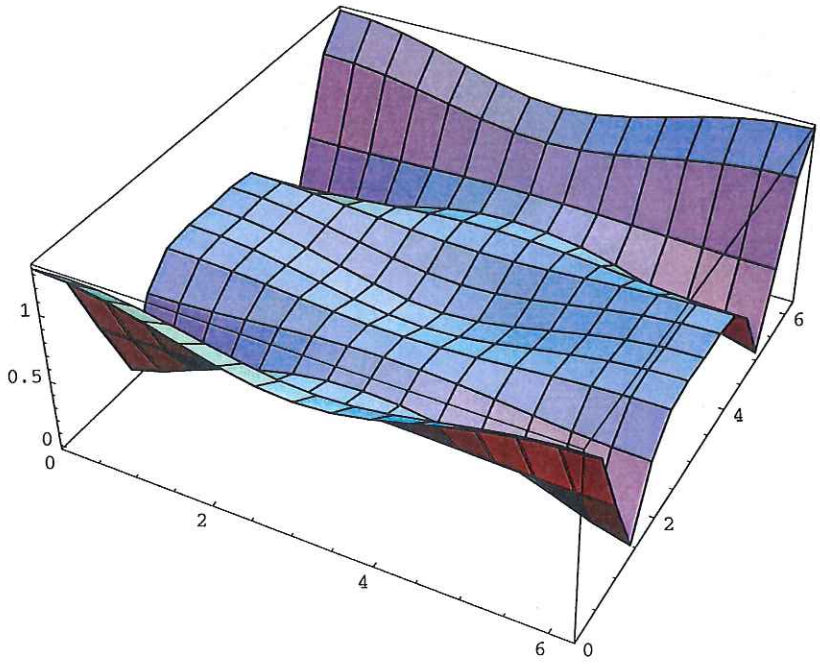


Figure 5.15: A plot of radial length $\rho$ versus $y$ and $z$ for the first eigenmode.

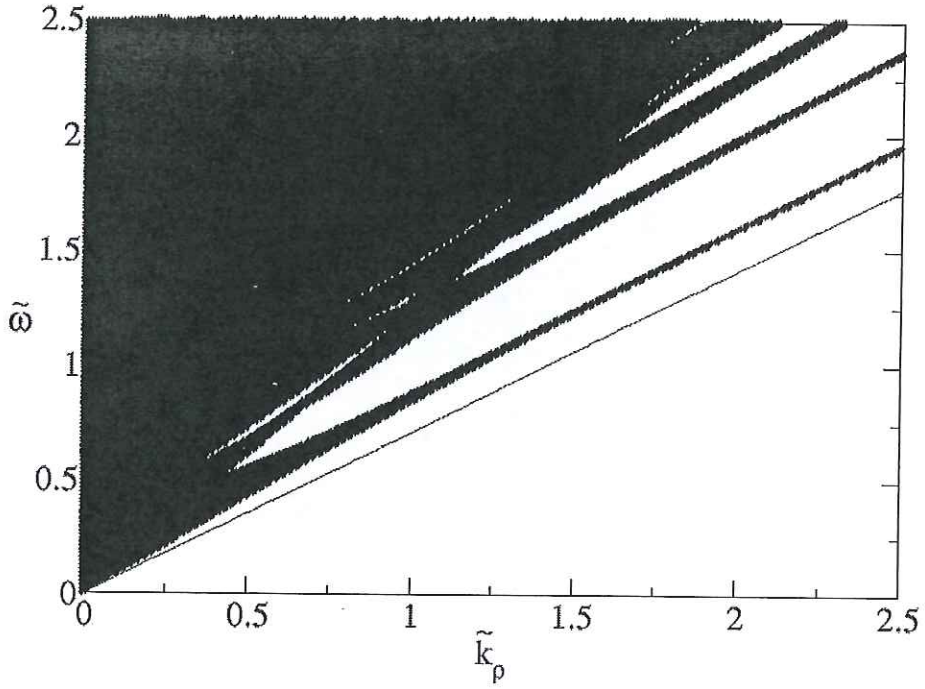


Figure 5.16: Omnidirectional band structure diagram for an ideal helix. Shaded regions correspond to allowed modes, while white regions correspond to forbidden modes. The red line represents a naïve lower bound on $\tilde{\omega}$. States with $\tilde{k}_\rho = 0$ correspond to normal incidence, whereas states near the red line correspond to highly oblique (nearly grazing) incidence.

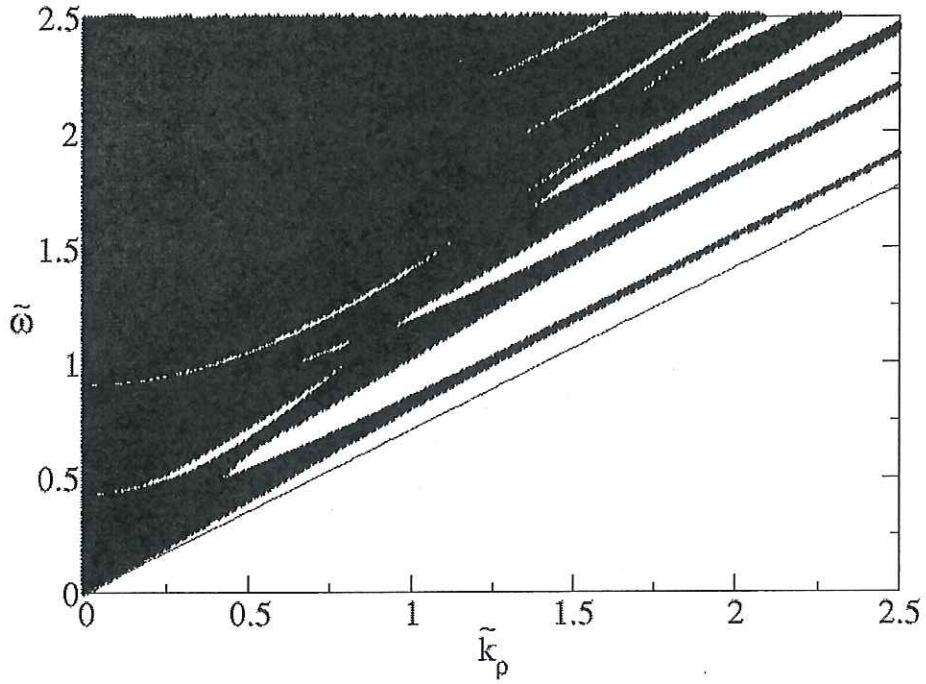


Figure 5.17: Omnidirectional band structure for a distorted helix ($e = 0.1$, $r = 1.9$).

# Chapter 6

# Conclusions

In this thesis, I have reviewed the mechanical properties of a cholesteric elastomer, and have developed two methods to calculate how stretching will affect the underlying optical properties – de Vries' technique and the more modern band structure approach. However, most of the results are calculated using the band structure approach, because of its greater versatility. At normal incidence, de Vries finds a single gap for one polarisation. It is also found that stretching gives rise to gaps at multiple Brillouin zone boundaries, which scale as power laws of the strain, for small strains. The scaling exponents can be calculated by combining second-order degenerate perturbation theory with numerical results for the scaling of the Fourier components, $c_n$ and $s_n$. The lower gaps have a lower exponent and are thus much larger. Interestingly, a gap also opens up for the opposite handedness of light, which represents a decrease in the circular dichroism. This phenomenon can be explained in the context of de Vries' approach by the fact that the helix twists back and forth in the rotating frames of both handednesses upon stretching. I can also calculate the optical properties of a helix at oblique incidence. However, interpreting the data is more challenging than for normal incidence, due to the refraction which occurs at boundaries as well as the non-trivial relationship between polarisation and dispersion relations. Fortunately, the omnidirectional band structure successfully summarises the experimental situation of interest, by predicting what happens to light of a given frequency and angle of incidence. Following a line with a particular slope corresponds to an experiment that takes place at a specific angle of incidence outside the medium. It is evident that there are many Bragg-like reflections which are spaced more widely apart at larger angles. Ultimately, at grazing incidence, no Bragg reflections occur, and the dispersion grows with the magnitude of $\mathbf{k}$ (which in the higher bands, may include a reciprocal lattice vector).

Several experiments support these conclusions. Finkelmann's experiments with cholesteric elastomers have shown that the optical properties change with mechanical deformation. The frequencies reflected at normal incidence increase with stretching, as predicted [6].

Furthermore, a loss of circular dichroism corresponding to a cross-over at a deformation $\lambda_c$ is observed after leaving the sample overnight [22]. Finally, the frequencies reflected at a particular harmonic have been experimentally shown to increase with an increase in the angle of incidence [41].

The most immediate application of these results is in the field of cholesteric lasing, which has already been successfully demonstrated in experiments [5, 37, 6]. It explains how modes just above the first band edge in an ideal helix are able to lase – as is evident from the omnidirectional band structures, they are forbidden beyond a small angle away from normal, which keeps them collimated. This work gives detailed results that may be used to tune the lasing frequencies and modes in non-trivial ways using relatively simple materials. Such tunable lasing technology, in turn, may prove important in applications such as telecommunications and industry.

# Bibliography


[1] R. D. Meade, K. D. Brommer, A. M. Rappe, and J. Joannopoulos, Phys. Rev. B **44**, 13772 (1991).

[2] E. Yablonovitch, Phys. Rev. Lett. **58**, 2059 (1987).

[3] O. Painter *et al.*, Science **284**, 1819 (1999).

[4] J. Dowling, M. Scalora, M. Bloemer, and C. Bowden, J. Appl. Phys. **75**, 1896 (1994).

[5] V. Kopp, B. Fan, H. Vithana, and A. Genack, Opt. Lett. **23**, 1709 (1998).

[6] P. Palffy-Muhoray *et al.*, submitted to Adv. Mater. (unpublished).

[7] S. Barnes, Telecommunications International **8**, (2001).

[8] S. John, Phys. Rev. Lett. **53**, 2169 (1984).

[9] S. John, Phys. Rev. Lett. **58**, 2486 (1987).

[10] E. Yablonovitch and T. Gmitter, Phys. Rev. Lett. **63**, 1950 (1989).

[11] K. Ho, C. Chan, and C. Soukoulis, Phys. Rev. Lett. **65**, 3152 (1990).

[12] K. Leung and Y. Liu, Phys. Rev. Lett. **65**, 2646 (1990).

[13] Z. Zhang and S. Satpathy, Phys. Rev. Lett. **65**, 2650 (1990).

[14] E. Yablonovitch, T. Gmitter, and K. Leung, Phys. Rev. Lett. **67**, 2295 (1991).

[15] E. Ozbay *et al.*, Phys. Rev. B **50**, 1945 (1994).

[16] J. Wijnhoven and W. Vos, Science **281**, 802 (1998).

[17] A. Urbas, Y. Fink, and E. Thomas, Macromolecules **32**, 4748 (1999).

[18] M. Muller *et al.*, Adv. Mater. **12**, 1499 (2000).

[19] H. de Vries, Acta Cryst. **4**, 219 (1951).

[20] P. de Gennes and J. Prost, *The Physics of Liquid Crystals* (Clarendon Press, Oxford, 1993).

[21] H. Finkelmann, H. Koch, and G. Rehage, Macromol. Rapid Commun. **2**, 317 (1981).

[22] S. Kim and H. Finkelmann, submitted to Macromol. Rapid Comm. (in press) (unpublished).

[23] M. Warner, E. Terentjev, R. Meyer, and Y. Mao, Phys. Rev. Lett. **85**, 2320 (2000).

[24] R. Meade *et al.*, Phys. Rev. B **48**, 8434 (1993).

[25] P. Chaiken and T. Lubensky, *Principles of Condensed Matter Physics* (Cambridge University Press, Cambridge, U.K., 1995).

[26] S. Chou, L. Cheung, and R. Meyer, Solid State Comm. **11**, 277 (1972).

[27] R. Meyer, Appl. Phys. Lett. **12**, 281 (1968).

[28] P. de Gennes, Solid State Comm. **6**, 163 (1968).

[29] R. Meyer, Appl. Phys. Lett. **14**, 208 (1969).

[30] I. Bronshtein and K. Semendyayev, *Handbook of Mathematics* (Van Nostrand-Reinhold, New York, NY, 1985).

[31] L. Treloar, *The Physics of Rubber Elasticity* (Clarendon Press, Oxford, 1975).

[32] K. Huang, *Statistical Mechanics* (John Wiley and Sons, New York, 1987).

[33] A. R. Tajbakhsh and E. M. Terentjev, submitted to LANL preprint archive, available at http://xxx.lanl.gov/abs/cond-mat/0106138 (unpublished).

[34] E. Terentjev, J. Phys.: Condens. Matter **11**, R239 (1999).

[35] P. D. Olmsted, J. Physique II **4**, 2215 (1994).

[36] D. Berreman and T. Scheffer, Phys. Rev. Lett. **25**, 577 (1970).

[37] V. Kopp and A. Genack, in *Photonics West SPIE Conference on Organic Photonic Materials and Devices* (PUBLISHER, ADDRESS, 1999).

[38] E. Anderson *et al.*, *LAPACK: A Portable Linear Algebra Library for High Performance Computers* (SIAM Publications, Philadelphia, 1995).

[39] S. Johnson and J. Joannopoulos, Optics Express **8**, 173 (2001).

[40] Y. Fink *et al.*, Science **282**, 1679 (1998).

[41] H. Takezoe *et al.*, Jap. J. Appl. Phys. **22**, 1080 (1983).